Electronic structure calculations of liquid-solid interfaces: Combination of density functional theory and modified Poisson-Boltzmann theory

Ryosuke Jinnouchi and Alfred B. Anderson
Department of Chemistry, Case Western Reserve University, 10900 Euclid Avenue, Cleveland, Ohio 44106-7078, USA
(Received 30 March 2008; revised manuscript received 29 April 2008; published 12 June 2008)

A robust and efficient computational method for electronic structure calculations of liquid-solid interfaces is presented. The theory employs the density functional theory and a modified Poisson-Boltzmann theory, combining them through a smooth dielectric model function. The free energy, including electrostatic and nonelectrostatic interactions between solutes and the solvation medium, is formulated, and its first derivatives with atomic positions are presented. This methodology is applied to two different topics; one is the potential of zero charge (PZC) of Pt(111), and the other is a poisoning of active sites for the oxygen-reduction reaction (ORR) by interfacial water molecules on Pt(111). The results of the first topic show that induced charge redistributions caused by the adsorption of water molecules form a surface dipole moment that dominates the experimentally observed negative shift in the PZC when platinum is immersed in an aqueous electrolyte. The results of the second topic show the possibility of a decrease in the surface coverage of the first reaction precursor to the ORR due to site blocking by the adsorbed water molecules.

DOI: 10.1103/PhysRevB.77.245417 PACS number(s): 71.15.Nc, 73.20.At, 73.20.Hb

I. INTRODUCTION

Recent progresses in first principle calculations with the density functional theory (DFT)[1,2] allow one to quantitatively predict wide varieties of electrochemical properties; however, it is still a very challenging task to accurately predict the Gibbs free energies of liquid-solid interfaces under given electrode potentials, which is a practically important technique for computer aided designing of new active and corrosive-resistant electrocatalysts for fuel cells, as well as for attaining a fundamental understanding of surface electrochemistry. This difficulty comes from the necessity to include both accurate descriptions of local chemical bonds and long range disordered structures of electric double layers. Although DFT calculations using slab models with periodic boundary conditions have reproduced bond strengths between adsorbates and surfaces in a vacuum within useful accuracies, it is not practical to perform *ab initio* molecular dynamics on a system with a scale of 100 Å, which is the typical length needed for the sufficient screening of the electrostatic field from a charged surface in a 0.1*M* aqueous solution. Therefore, actual calculations need approximations.

As an example, we present the approximations used in previous studies for predictions of the redox potentials of electron transfer reactions at interfaces,

$$A(\mathrm{ads}) + ne^- \leftrightarrow B(\mathrm{ads}). \tag{1}$$

The Gibbs free energy of electrons is $-neU$, where e is the elementary electric charge and U is the electrode potential. The Gibbs free energies of A(ads) and B(ads) are functions of U, which we denote as $\Omega_{A(\mathrm{ads})}$ and $\Omega_{B(\mathrm{ads})}$, respectively. The free energy change before and after the reaction is zero at the redox potential U^0,

$$-neU^0 + \Omega_{A(\mathrm{ads})}(U^0) = \Omega_{B(\mathrm{ads})}(U^0). \tag{2}$$

This is the general equation to be solved; however, it is difficult to accurately represent $\Omega_{A(\mathrm{ads})}$ and $\Omega_{B(\mathrm{ads})}$.

This laboratory has developed a simple approach using a relationship between reaction internal energies and reaction free energies discovered in 1999.[3] First, this method approximates $\Omega_{A(\mathrm{ads})}$ and $\Omega_{B(\mathrm{ads})}$ as the free energies of the same species on the neutral surface. Second, thermal corrections to internal energies, entropies, and solvation free energies are approximated by those in an aqueous solution. A simple equation is derived from these approximations as

$$U^0 \cong -\frac{\Delta E_B - \Delta E_A}{ne} - \frac{\Omega_{B(\mathrm{aq})} - \Omega_{A(\mathrm{aq})}}{ne} = -\frac{\Delta\Delta E_r}{ne} + U^0_{\mathrm{aq}}. \tag{3}$$

ΔE_A and ΔE_B are the differences in internal energies caused by transferring A and B, respectively, from the solution to the neutral surface. $\Omega_{A(\mathrm{aq})}$ and $\Omega_{B(\mathrm{aq})}$ are the free energies of A and B, respectively, in the solution. U^0_{aq} is the redox potential in the solution. $\Delta\Delta E_r$ was obtained from DFT calculations using slab models or cluster models, and U^0_{aq} was taken from experimental data. Nørskov *et al.*[4] developed useful kinetic models to predict the activities of electrocatalysts for the hydrogen evolution reaction and the oxygen-reduction reaction[5] (ORR) using similar approximations. The differences are that they did not use the experimental aqueous redox potential U^0_{aq} but instead used the Gibbs free energies that were approximately calculated from internal energies and zero point energies on neutral surfaces. Although these methods have given useful predictions for redox potentials,[6–28] catalytic activities,[29–32] and phase diagrams[33] consistent with experiments, limitations and unanswered questions remain. For example, these two models cannot include the potential dependencies of bond strengths into calculations. Structures and stabilities of water molecules are sensitive to the electrode potential,[34] and such potential dependencies may affect the activities of reactions as described in Sec. III of this paper. Another limitation is that these two models cannot give insights into well-established experimental measurements about charged surfaces, such as differential

capacitances and electrocapillarities.[35] Rossmeisl *et al.*[33] suggested the use of a constant electric field model using a neutral surface system including a dipole sheet for modeling of the interface between the charged surface and the solution. However, it is questionable that to apply a constant electric field to the neutral surface is a correct model for the actual charged surface in the electric double layer, and assumptions of the thickness of the double layer and the reference electrode potential used for the estimation of the electrode potential present additional uncertainties. Such measurements have played essential roles in obtaining microscopic information for interfaces, and comparisons between theories and experiments give further knowledge about surface electrochemistry, as well as validations of state-of-the-art models used in electronic structure calculations. In addition to these limitations, there is a question about the accuracies of solvation free energies. Solvation free energies are statistically averaged interactions between solutes and solutions. A few dozen up to several hundred water molecules have been used for the modeling of solvation, and sufficient statistical averages have been performed in molecular theories.[36–41] Otherwise, continuum solvation models, such as the polarizable continuum model (PCM),[42–44] the conductorlike screening model (COSMO),[45] or the solvation model (SM*x*),[46,47] have been used for the accurate evaluations of solvation free energies. However, just a few water molecules or a few layers of water molecules were used without any statistical average in a previous work that modeled the electrochemical interface.

In order to include surface charging effects into calculations, a direct solution of Eq. (2) is necessary. Lozovoi *et al.*[48] and Lozovoi and Alavi[49] developed a useful approach using slab models and applied it to the predictions of the phase transitions for Pt(110) and Au(110) surfaces. Neurock and co-workers[50–54] developed a more advanced interfacial model for the calculations of electrochemical reactions in fuel cells. In these methods, the internal energies and Fermi energies of systems before and after the reaction with different electron numbers are obtained from DFT calculations. The Fermi energies are transformed into the electrode potential within the standard hydrogen electrode (SHE) scale by using the experimental thermodynamic work function for the SHE. Then, the internal energies as functions of the electrode potential are interpolated by quadratic interpolations. Finally, the redox potential is calculated as an intersecting point between two curves. Recently, Sugino *et al.*[55] also applied a similar model for an investigation of the structure of water on the Pt(111) surface using a molecular dynamics method. However, there are still questions about these methodologies. One question is about the arbitrariness in countercharge distributions. In order to handle the charged surfaces by DFT calculations with periodic boundary conditions, countercharges neutralizing the system must be introduced. Two simple methods have been employed: the Gaussian charge sheets of Lozovoi and Alavi[49] and the homogeneous background charge of Neurock and co-workers.[50–54] The actual ion distributions must be functions of the ion concentration in the solution as shown in the Gouy–Chapman theory.[56,57] The Gaussian charge sheets or the homogeneous background charge can only qualitatively represent such dependence by changing the distances between the surface and charge sheets or by changing the size of the translational unit cell. However, it is difficult to quantitatively relate the distance or the size to the ion concentration without *ad hoc* assumptions. In order to avoid using these artificial treatments for countercharges, Skúlason *et al.*[58] proposed to control the electrode potential by changing not only the number of electrons but also the number of hydrogen atoms to keep the net charge neutral and applied it to the calculations of activation energies for the Heyrovsky reaction. However, another question regarding the lack of interactions from a long ranged electric double layer remains. Furthermore, adding or removing one electron and one hydrogen atom to or from the practically available small unit cells causes a drastic change in the calculated electrode potential by ± 1.0 V; therefore, it is quite difficult to control the electrode potential within a desired narrow range. In addition, the question on the accuracies of solvation free energies remains.

Recently, Otani and Sugino[61] proposed to combine the DFT and a modified Poisson-Boltzmann theory (MPB)[59,60] to get more realistic ion distributions. The basic idea is close to that in PCM,[43,45] COSMO,[46] or SM*x*.[46,47] A cavity is created in the dielectric medium, and a slab is placed in the cavity. The electrostatic potential and ion distributions are determined by using the MPB, and the electronic structure of the slab is determined by using the DFT. However, the treatments for the interface between the region handled by the DFT and the region handled by the MPB are too primitive to accurately describe solute-solvent interactions.

Recently, we developed a model combining the DFT and the MPB and demonstrated its ability to predict with a useful accuracy the reversible potentials for 38 electron transfer reactions in acid and base aqueous solutions and on Pt(111) in an acid aqueous medium.[62] In this model, the DFT and MPB are combined through a smooth and flexible dielectric model function.[63–65] In this paper, we present the details of this model. The free energy, including cavitation, dispersion, and repulsion contributions, is presented. Its derivatives with atomic positions are formulated. We implemented all these methods into a newly developed computational code using linear combinations of pseudoatomic orbitals (LCPAOs) and norm-conserving pseudopotentials. We applied this method to two different topics; one is the potential of zero charge (PZC) of the Pt(111) surface, and the other is a poisoning of the active sites for the ORR on the Pt(111) surface due to surface blocking by interfacial water molecules. In the first topic, the theory gives a mechanism for explaining the experimentally observed negative shift of the PZC by solvation. In the second topic, the theory shows the possibility of a significant decrease in the surface coverage of a reaction precursor in the important range of the electrode potential for the ORR. In Sec. II, we introduce the basic equations and methods for the implementation to a DFT code along with the details of the models and computations. In Sec. III, we present the results and discussion. A summary of this work is described in Sec. IV.

II. THEORY

A. Free energy and its derivatives

In this work, we combine the DFT and the MPB. In this approach, a cavity is created in the system, and solutes or

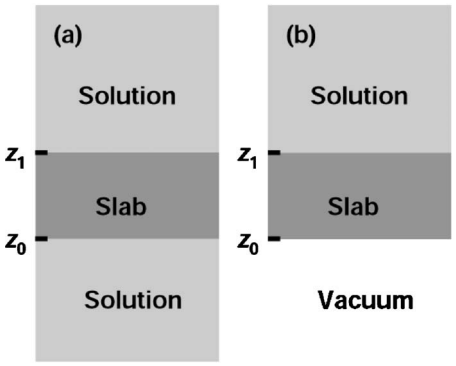

FIG. 1. Schematic of models: (a) a slab sandwiched by solvation mediums and (b) a slab sandwiched by the solvation medium and the vacuum. z_0 and z_1 denote the positions of the nucleus in the bottom and top layers, respectively, of the slab.

surfaces are placed in the cavity. We include two different boundary conditions for modeling interfaces. One is solution/slab/solution, and the other is vacuum/slab/solution [see Figs. 1(a) and 1(b)]. The total free energy of the system is formulated as

$$\Omega_{\text{tot}} = K + E_{\text{xc}} + E_{\text{es}} + \Omega_{\text{ss,nonel}} + \Omega_{\text{is,nonel}} - TS_e - TS_i + H_{s,\text{corr}} - TS_s + \Omega_{\text{mc}}. \quad (4)$$

K, E_{xc}, and E_{es} are the kinetic, exchange-correlation, and electrostatic energies, respectively. $\Omega_{\text{ss,nonel}}$ and $\Omega_{\text{is,nonel}}$ are the respective free energies due to nonelectrostatic solute-solvent and ions-solute interactions, $H_{s,\text{corr}}$ are the thermal corrections to the enthalpy for the solute, T is the temperature, and S_e, S_i, and S_s are the respective entropies of the electrons, ions, and solutes. In this study, we set the temperature to 298.15 K. Ω_{mc} is the mass conservation term.

K is written as

$$K = \sum_{\sigma} \sum_{\mathbf{k}} \sum_{i} f_{i\mathbf{k}\sigma} \int d\mathbf{r}\, \psi^*_{i\mathbf{k}\sigma}(\mathbf{r}) \left(-\frac{1}{2}\nabla^2 \right) \psi_{i\mathbf{k}\sigma}(\mathbf{r}). \quad (5)$$

$f_{i\mathbf{k}\sigma}$ and $\psi_{i\mathbf{k}\sigma}$ denote the occupation numbers and wave functions for the ith band index for point $\mathbf{k}$ in the Brillouin zone and σ spin state. All integrals without any notation mean integrals within the translational unit cell. We applied a generalized gradient approximation (GGA) by using the revised Perdew–Burke–Ernzerhof (RPBE) functional developed by Hammer *et al.*[66] Several calculations were also performed using the Perdew–Burke–Ernzerhof (PBE) functional.[67] The exchange-correlation energy is given by

$$E_{\text{xc}} = E_{\text{xc}}[\rho_\uparrow, \rho_\downarrow] = \int d\mathbf{r} f_{\text{xc}}(\rho_\uparrow, \rho_\downarrow, \nabla\rho_\uparrow, \nabla\rho_\downarrow). \quad (6)$$

ρ_σ is the density of electrons with spin σ,

$$\rho_\sigma(\mathbf{r}) = \sum_{\mathbf{k}} \sum_{i} f_{i\mathbf{k}\sigma} |\psi_{i\mathbf{k}\sigma}(\mathbf{r})|^2. \quad (7)$$

The electrostatic energy E_{es} is written as

$$E_{\text{es}} = \int d\mathbf{r}[\rho_e(\mathbf{r}) + \rho_c(\mathbf{r}) + \rho_-(\mathbf{r}) + \rho_+(\mathbf{r})]\phi(\mathbf{r}) - \int d\mathbf{r} \frac{\varepsilon(\mathbf{r})}{8\pi} |\nabla\phi(\mathbf{r})|^2. \quad (8)$$

ρ_e is the charge density of electrons,

$$\rho_e(\mathbf{r}) = \sum_{\sigma} \rho_\sigma(\mathbf{r}). \quad (9)$$

ρ_c, ρ_-, and ρ_+ are the charge densities for nuclei, anions, and cations, respectively. ϕ is the electrostatic potential. The sign for the charge density of electrons is defined as positive in this work. The relative permittivity ε is a position-dependent function written as follows:

$$\varepsilon(\mathbf{r}) = 1 + \frac{\varepsilon_\infty(\mathbf{r}) - 1}{2} \left\{ 1 + \frac{1 - [\rho_{\text{na}}(\mathbf{r})/\rho_0]^{2\beta}}{1 + [\rho_{\text{na}}(\mathbf{r})/\rho_0]^{2\beta}} \right\}. \quad (10)$$

ρ_{na} is a summation of neutral atomic electron densities and is written as

$$\rho_{\text{na}}(\mathbf{r}) = \sum_{\mathbf{R}} \sum_{\alpha=1}^{N_{\text{atom}}} \rho_{\text{na},\alpha}(|\mathbf{r} - \mathbf{R}_\alpha - \mathbf{R}|), \quad (11)$$

where $\rho_{\text{na},\alpha}$ denotes the electron density of the atom calculated with the central field approximation, $\mathbf{R}_\alpha$ denotes the position of the atom, and $\mathbf{R}$ denotes lattice vectors. Equation (10) approaches ε_∞ in the regions where the electron density is low and 1 in the regions where the electron density is high. The parameter ρ_0 is the density threshold that determines the cavity size, and the parameter β controls the smoothness of the transition from ε_∞ to 1. ε_∞ is a position-dependent function written as

$$\varepsilon_\infty(\mathbf{r}) = \begin{cases} \varepsilon_b & \text{for system a} \\ -\dfrac{\varepsilon_b - 1}{2} \left[1 - \text{erf}\left(\dfrac{z - z_0}{\Delta_z} \right) \right] + \varepsilon_b & \text{for system b,} \end{cases} \quad (12)$$

where z_0 is taken as the z position of the bottom of the slab and Δ_z is taken as a small value. We set Δ_z as 1 Å in this study. In the case of system a, Eq. (10) is the same as the model suggested by Fattebert and Gygi[63,64] except that it does not use ρ_e but ρ_{na}. We discovered that using ρ_{na} instead of ρ_e gives more accurate solvation free energies for both H^+ and OH^-. The solvation free energies of H^+ and OH^- were calculated as the changes in the free energies for the reactions $H^+(g) + (H_2O)_4(aq) \rightarrow H^+(H_2O)_4(aq)$ and $OH^-(g) + (H_2O)_3(aq) \rightarrow OH^-(H_2O)_3(aq)$, respectively. The best solvation free energies were −12.11 and −4.75 eV for H^+ and OH^-, respectively, in the case of the method using ρ_e and −11.36 and −4.98 eV for H^+ and OH^-, respectively, in the case of the method using ρ_{na}. The experimental values are -11.44 ± 0.1 and -4.64 ± 0.1 eV for H^+ and OH^-, respectively, as summarized in Ref. 47. The experimental solvation free energies of these ions are still controversial issues, but using ρ_{na} apparently gives a better free energy difference for the reaction $H_2O(aq) \rightarrow H^+(aq) + OH^-(aq)$. The method using ρ_e gives 0.20 eV, and the method using ρ_{na} gives 0.72 eV.

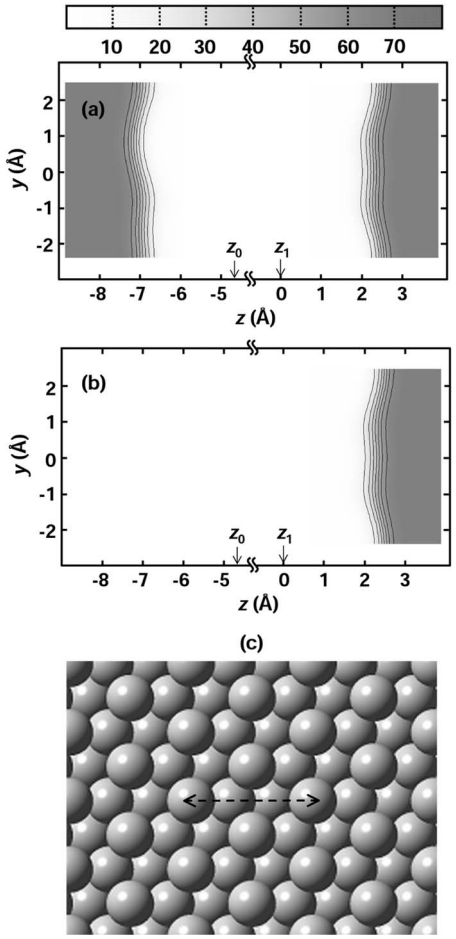

FIG. 2. Distributions of relative permittivity ε for (a) a slab sandwiched by solvation mediums and (b) a slab sandwiched by the solvation medium and the vacuum and (c) the top view of the slab. The distributions are on the cross section shown as a dotted arrow in (c). The line spacing of the contour plot is 10. z_0 and z_1 denote the positions of the nucleus in the bottom and top layers, respectively, of the slab.

The experimental value is 0.93 eV. Our impression is that the method using ρ_e overestimates the solvation free energies for cations. In addition to this advantage, we found that using ρ_{na} can decrease the needed number of grids for numerical solutions of the Poisson equation. We introduced the new position-dependent function for ε_∞ in order to apply the similar methodology to system b: ε_∞ approaches 1 for $z \ll z_0$ and ε_b for $z \gg z_0$. We set ε_b to 78.36, which is the relative permittivity of liquid water at 298.15 K.[68] Figures 2(a) and 2(b) show the relative permittivity distributions for a Pt(111) surface modeled by a three-layer slab in the aqueous solution. The distributions are on a cross section shown as a dotted arrow in Fig. 2(c).

$\Omega_{\mathrm{ss,nonel}}$ includes the cavitation, dispersion, and repulsion free energies as follows:

$$\Omega_{\mathrm{ss,nonel}} = \Omega_{\mathrm{ss,cav}} + \Omega_{\mathrm{ss,dr}} + \Omega_{\mathrm{ss,rep}}. \tag{13}$$

For the cavitation free energy, we used the following phenomenological equation:

$$\Omega_{\mathrm{ss,cav}} = \gamma_b S. \tag{14}$$

γ_b is the surface tension of the bulk solution, and we used 71.99 mN/m for liquid water at 298.15 K.[69] S is the surface area of the solute or the slab numerically calculated using the following equations:

$$S = \int d\mathbf{r} s(\rho_{\mathrm{na}}, |\nabla \rho_{\mathrm{na}}|), \tag{15}$$

$$s(\rho_{\mathrm{na}}, |\nabla \rho_{\mathrm{na}}|) = \xi(\mathbf{r})[\vartheta_{\rho_0-\Delta/2}(\mathbf{r}) - \vartheta_{\rho_0+\Delta/2}(\mathbf{r})] \times \frac{|\nabla \rho_{\mathrm{na}}(\mathbf{r})|}{\Delta}, \tag{16}$$

$$\xi(\mathbf{r}) = \begin{cases} 1 & \text{for system a} \\ -\frac{1}{2}\left[1 - \mathrm{erf}\left(\frac{z - z_0}{\Delta_z}\right)\right] + 1 & \text{for system b,} \end{cases} \tag{17}$$

$$\vartheta_{\rho_0}(\rho_{\mathrm{na}}) = \frac{1}{2}\left\{\frac{[\rho_{\mathrm{na}}(\mathbf{r})/\rho_0]^{2\beta} - 1}{[\rho_{\mathrm{na}}(\mathbf{r})/\rho_0]^{2\beta} + 1} + 1\right\}. \tag{18}$$

We used 0.0002 a.u. for Δ. Equations (14)–(18) for system a are same as those proposed by Scherlis *et al.*[65] except that ρ_{na}

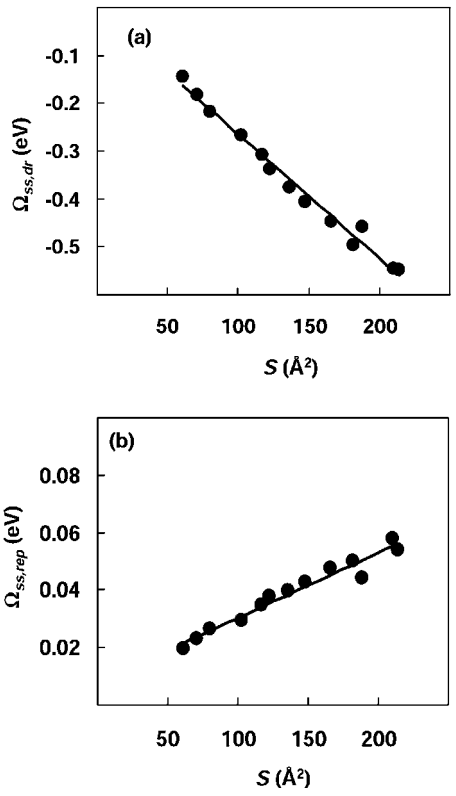

FIG. 3. Free energies for nonelectrostatic interactions as functions of the surface area of solutes, $S(\text{Å}^{-2})$, (a) dispersion free energies, $\Delta\Omega_{\mathrm{SS,dr}}$ (eV), and (b) repulsion free energies, $\Delta\Omega_{\mathrm{SS,rep}}$ (eV). The circles are the free energies given from GAUSSIAN03. The solid lines are the fitted free energies to the circles.

is included in our method. We introduced a new position-dependent function ξ for applying the methodology to system b. Taking into account empirical relationships between dispersion and repulsion free energies and the solute surface area,[70–72] we formulated these free energies as

$$\Omega_{\mathrm{ss,dr}} + \Omega_{\mathrm{ss,rep}} = \sum_{\alpha=1}^{N_{\mathrm{atom}}} (a_\alpha S_\alpha + b_\alpha). \tag{19}$$

The coefficients a_α and b_α are atom-dependent parameters. The surface areas of atoms are calculated by a partitioning method,[73]

$$S_\alpha = \int d\mathbf{r} p_\alpha(\mathbf{r}) s(\rho_{\mathrm{na}}, |\nabla \rho_{\mathrm{na}}|). \tag{20}$$

The function p_α is the partition function, and we used the form proposed by Delley:[74]

$$p_\alpha(\mathbf{r}) = \frac{\sum_{\mathbf{R}} f_\alpha(|\mathbf{r} - \mathbf{R}_\alpha - \mathbf{R}|)}{\sum_{\mathbf{R}} \sum_{\beta}^{N_{\mathrm{atom}}} f_\beta(|\mathbf{r} - \mathbf{R}_\beta - \mathbf{R}|)}, \tag{21}$$

$$f_\alpha(r) = \frac{\rho_{\mathrm{na},\alpha}(r)}{r^2}. \tag{22}$$

The parameters a_α and b_α were fitted to give the same dispersion and repulsion interactions as those calculated by the PCM model implemented in GAUSSIAN03.[75] In this study, we used the same parameters for all atoms. Figures 3(a) and 3(b) show the dispersion and repulsion free energies of several clusters including $(H_2O)_n$, $H^+(H_2O)_n$, and $OH^-(H_2O)_n$ calculated by GAUSSIAN03 as functions of the surface area using Eq. (15). The fitted parameters reproduce dispersion and repulsion free energies within a mean absolute difference of 0.015 eV.

We introduced an interaction model for the free energy $\Omega_{\mathrm{is,nonel}}$ in order to represent the Helmholtz layer,

$$\Omega_{\mathrm{is,nonel}} = \int d\mathbf{r}(|\rho_-(\mathbf{r})| + |\rho_+(\mathbf{r})|)\phi_{\mathrm{rep}}(\mathbf{r}), \tag{23}$$

$$\phi_{\mathrm{rep}}(\mathbf{r}) = \sum_{\mathbf{R}} \sum_{\alpha}^{N_{\mathrm{atom}}} u_\alpha(|\mathbf{r} - \mathbf{R}_\alpha - \mathbf{R}|). \tag{24}$$

u_α is the repulsive interaction from the atom, and we used a repulsive interaction function written as

$$u_\alpha(r) = \begin{cases} \infty, & r \le r_\alpha - \Delta_{\mathrm{rep}} \\ \dfrac{e^{-2\Delta_{\mathrm{rep}}/(r_\alpha + \Delta_{\mathrm{rep}} - r)}}{r - r_\alpha + \Delta_{\mathrm{rep}}}, & r_\alpha - \Delta_{\mathrm{rep}} < r \le r_\alpha + \Delta_{\mathrm{rep}} \quad \text{for system a} \\ 0, & r_\alpha + \Delta_{\mathrm{rep}} \le r \\ \infty, & r \le r_\alpha - \Delta_{\mathrm{rep}} \text{ and } z \le z_0 \\ \dfrac{e^{-2\Delta_{\mathrm{rep}}/(r_\alpha + \Delta_{\mathrm{rep}} - r)}}{r - r_\alpha + \Delta_{\mathrm{rep}}}, & r_\alpha - \Delta_{\mathrm{rep}} < r \le r_\alpha + \Delta_{\mathrm{rep}} \text{ and } z > z_0 \quad \text{for system b,} \\ 0, & r_\alpha + \Delta_{\mathrm{rep}} \le r \text{ and } z > z_0 \end{cases} \tag{25}$$

where r_α is the average solvated ion radius a, which was set as 3 Å in this study, and the van der Waals radius of the atom. The Δ_{rep} parameter is for softening the potential and was set as 1 Å in this work.

We applied the MPB for a symmetric 1:1 electrolyte with an ion radius a developed by Borukhov *et al.*[59,60] This theory takes into account the finite size effects of ions and gives a simple form for the entropy of the solution as

$$\begin{aligned} S_{\mathrm{ion}} = -\frac{k_B}{a^3} \int d\mathbf{r} [&|\rho_+(\mathbf{r})|a^3 \ln(|\rho_+(\mathbf{r})|a^3) \\ &+ |\rho_-(\mathbf{r})|a^3 \ln(|\rho_-(\mathbf{r})|a^3) \\ &+ (1 - |\rho_+(\mathbf{r})|a^3 - |\rho_-(\mathbf{r})|a^3) \\ &\times \ln(1 - |\rho_+(\mathbf{r})|a^3 - |\rho_-(\mathbf{r})|a^3)], \end{aligned} \tag{26}$$

where k_B is Boltzmann's constant.

We applied the Methfessel–Paxton smearing technique with a Hermite polynomial of degree 2 to determine the occupation numbers of eigenstates.[76] The formula for S_e is given in Ref. 76, and we used a broadening parameter of 0.2 eV.

$H_{s,\mathrm{corr}}$ and S_s were approximately calculated by a simple statistical thermodynamic model.[77] In the case of adsorbed species, we applied thermal correction terms to enthalpies and entropies using the harmonic vibration model written as follows:

$$H_{s,\mathrm{corr}} = H_{\mathrm{vib}}, \tag{27}$$

$$S_s = S_{\mathrm{vib}}, \tag{28}$$

$$H_{\mathrm{vib}} = \frac{1}{2}\sum_i h\nu_i + \sum_i \frac{h\nu_i}{e^{h\nu_i/k_BT} - 1}, \tag{29}$$

$$S_{\mathrm{vib}} = k_B \sum_i \left[\frac{h\nu_i/k_BT}{e^{h\nu_i/k_BT}-1} - \ln(1-e^{-h\nu_i/k_BT}) \right], \tag{30}$$

where ν_i are the vibration frequencies of adsorbed species calculated from the numerically obtained Hessian matrix and h is Planck's constant. In the case of isolated molecules, translational, rotational, and vibration modes were taken into account as follows:

$$H_{s,\mathrm{corr}} = H_{\mathrm{trans}} + H_{\mathrm{rot}} + H_{\mathrm{vib}}, \tag{31}$$

$$S_s = S_{\mathrm{trans}} + S_{\mathrm{rot}} + S_{\mathrm{vib}}, \tag{32}$$

$$H_{\mathrm{trans}} = \frac{3}{2}k_BT, \tag{33}$$

$$H_{\mathrm{rot}} = \begin{cases} k_BT & \text{for linear molecules} \\ \frac{3}{2}k_BT & \text{for nonlinear molecules,} \end{cases} \tag{34}$$

$$S_{\mathrm{trans}} = k_B \left[\ln\left(\frac{2\pi m k_B T}{h^2} \right)^{3/2} \frac{k_BT}{p} + 1 + \frac{3}{2} \right], \tag{35}$$

$$S_{\mathrm{rot}} = \begin{cases} k_B \ln\left(\frac{T}{\sigma\Theta_z} + 1 \right) & \text{for linear molecules} \\ k_B \ln\left(\frac{\pi^{1/2}T^{3/2}}{\sigma\sqrt{\Theta_x\Theta_y\Theta_z}} + \frac{3}{2} \right) & \text{for nonlinear molecules,} \end{cases} \tag{36}$$

$$\Theta_{x,y,z} = \frac{h^2}{8\pi^2 I_{x,y,z} k_B}, \tag{37}$$

where m is the mass of the molecule, p is the pressure, σ is the rotational symmetry number, and $I_{x,y,z}$ are the moments of inertia. We set the pressure as 0.1 MPa. We neglected the contributions of configurational entropies to S_s.

When the system is opened for electrons and ions, we need the mass conservation term written as

$$\Omega_{\mathrm{mc}} = -\varepsilon_F N_e - \mu_+ N_+ - \mu_- N_-, \tag{38}$$

$$N_i = \int d\mathbf{r}\rho_i(\mathbf{r}) \quad \text{where} \quad i = e, +, \text{or} -, \tag{39}$$

where ε_F is the Fermi energy and $\mu_\pm$ are the chemical potentials for anions and cations in the bulk solution, calculated as follows:[59,60]

$$\mu_\pm = k_BT \ln \frac{c_b a^3}{1-2c_b a^3}. \tag{40}$$

c_b is the concentration of ions in the bulk solution, and we set it as $1M$ in this study.

Important physical properties are given from the local or ground minima of Eq. (4). $\psi_{i\mathbf{k}\sigma}$, ϕ, and $\rho_\pm$ at the ground state with given atomic positions are determined by the variation principle. A variation of Eq. (4) with $\psi_{i\mathbf{k}\sigma}$ gives the Kohn–Sham equation,

$$\hat{H}_\sigma \psi_{i\mathbf{k}\sigma}(\mathbf{r}) = \varepsilon_{i\mathbf{k}\sigma}\psi_{i\mathbf{k}\sigma}(\mathbf{r}), \tag{41}$$

$$\hat{H}_\sigma = -\frac{1}{2}\nabla^2 + \phi(\mathbf{r}) + v_{\mathrm{xc},\sigma}(\mathbf{r}), \tag{42}$$

$$v_{\mathrm{xc},\sigma}(\mathbf{r}) = \frac{\delta E_{\mathrm{xc}}}{\delta\rho_\sigma}. \tag{43}$$

A variation with ϕ gives the Poisson equation,

$$\nabla\cdot[\varepsilon(\mathbf{r})\nabla\phi(\mathbf{r})] = -4\pi[\rho_e(\mathbf{r}) + \rho_c(\mathbf{r}) + \rho_-(\mathbf{r}) + \rho_+(\mathbf{r})]. \tag{44}$$

Variations with $\rho_\pm$ give the modified Boltzmann distributions for ions,

$$\rho_\pm(\mathbf{r}) = \mp \frac{c_b e^{[\pm\phi(\mathbf{r})-\phi_{\mathrm{rep}}(\mathbf{r})]/k_BT}}{1-2a^3c_b+2a^3c_b\cosh[\phi(\mathbf{r})/k_BT]e^{-\phi_{\mathrm{rep}}(\mathbf{r})/k_BT}}. \tag{45}$$

A self-consistent solution of Eqs. (41)–(45) gives the ground state for $\psi_{i\mathbf{k}\sigma}$, ϕ, and $\rho_\pm$ at given atomic positions. We can use the analytical derivatives of Eq. (4) with respect to atomic positions $\mathbf{R}_\alpha$ for searching ground or local minima. The formulas for the derivatives are summarized as follows:

$$\nabla_{\mathbf{R}_\alpha}\Omega_{\mathrm{tot}} = -\mathbf{F}_{\mathrm{HF}} - \mathbf{F}_{\mathrm{Pulay}} - \mathbf{F}_{\mathrm{solv,nonel}}, \tag{46}$$

$$\mathbf{F}_{\mathrm{HF}} = -\int d\mathbf{r}\nabla_{\mathbf{R}_\alpha}\rho_c(\mathbf{r})\phi(\mathbf{r}), \tag{47}$$

$$\mathbf{F}_{\mathrm{Pulay}} = -\sum_\sigma\sum_{\mathbf{k}}\sum_i \int d\mathbf{r}[\nabla_{\mathbf{R}_\alpha}\psi^*_{i\mathbf{k}\sigma}(\mathbf{r})(\hat{H}-\varepsilon_{i\mathbf{k}\sigma})\psi_{i\mathbf{k}\sigma}(\mathbf{r}) + \psi^*_{i\mathbf{k}\sigma}(\mathbf{r})(\hat{H}-\varepsilon_{i\mathbf{k}\sigma})\nabla_{\mathbf{R}_\alpha}\psi_{i\mathbf{k}\sigma}(\mathbf{r})], \tag{48}$$

$$\mathbf{F}_{\mathrm{solv,nonel}} = \frac{1}{8\pi}\int d\mathbf{r}\nabla_{\mathbf{R}_\alpha}\rho_{\mathrm{na}}(\mathbf{r})\frac{d\varepsilon}{d\rho_{\mathrm{na}}}|\nabla\phi(\mathbf{r})|^2 - \int d\mathbf{r}\nabla_{\mathbf{R}_\alpha}\rho_{\mathrm{na}}(\mathbf{r})\frac{\delta\Omega_{\mathrm{ss,nonel}}}{\delta\rho_{\mathrm{na}}} - \int d\mathbf{r}(|\rho_-(\mathbf{r})| + |\rho_+(\mathbf{r})|)\nabla_{\mathbf{R}_\alpha}\phi_{\mathrm{rep}}(\mathbf{r}). \tag{49}$$

B. Implementation

We implemented all of the methodologies described in Sec. II A in a computational code newly developed in this laboratory. The basic features of the code without the solvation medium are similar to those of conventional codes.[78–81] A brief introduction of the basic techniques is presented here. This code uses norm-conserving pseudopotentials[82] with the fully separable Klienman–Bylander form.[83] We made pseudopotentials by using results from all-electron calcula-

tions including scalar relativity.[84] The reference states and cutoff radii for H, O, and Pt pseudopotentials are $1s^{0.9}(0.50)2p^{0.0}(0.50)$, $2s^{2.0}(1.08)2p^{3.5}(1.08)3d^{0.0}(1.08)$, and $5d^{9.0}(1.20)6s^{0.0}(2.00)6p^{0.0}(2.40)5f^{0.0}(2.40)$, respectively, where the values in the parentheses are the cutoff radii in Bohr units. We used the $2p$ and $3d$ states as the local pseudopotentials for H and O. The electrostatic potential of a model charge proposed by Soler *et al.*[79] was used as the local pseudopotential for Pt. The partial core corrections[85] (PCCs) were taken into account for O and Pt. The cutoff radii for the PCCs are 0.37 and 1.18 in Bohr units for O and Pt, respectively. We applied the projector expansion technique developed by Ozaki and Kindo[81] in order to decrease numerical integration grids. We used 5 as the maximum angular momentum number and 4 as the number of radial projectors. The wave functions $\psi_{i\mathbf{k}\sigma}$ were expanded by the LCPAO method. We used optimized double zeta plus polarization (DZP) basis sets by using a scheme similar to the one suggested by Soler *et al.*[78] The cutoff radius of 8 Å was applied for the construction of the basis sets. The DZP basis set for H includes two radial functions for $1s$ and one radial function for $2p$. The DZP basis set for O includes two radial functions each for $2s$ and $2p$ and one radial function for $3d$. The DZP basis set for Pt includes two radial functions each for $5d$ and $6s$ and one radial function for $6p$. We did not take into account basis set superposition errors in this study. A combination of three-dimensional numerical integrations[73] and momentum space integrations[79] was used for calculating Hamiltonian and overlap matrix elements. For the three-dimensional numerical integrations, we applied the T2-type Chebyshev quadrature with the M3-type mapping function for radial integrations[86] and Lebedev grids for angular integrations.[87,88] The numbers for the radial grids were 22, 32, and 28 and the numbers for the angular grids were 110, 110, and 194 for H, O, and Pt, respectively. Using these integration grids with the projector expansion achieved a good convergence in the total energy within the order of 0.000 01 a.u.. The current code can handle isolated molecules, slabs with two-dimensional periodic boundary conditions, and bulk crystals with three-dimensional periodic boundary conditions. The electrostatic potential was calculated by combinations of decompositions of electron densities to multipolar components and Ewald summation methods.[89–91] The integration grids described above were used for the decompositions of electron densities.

We reorganize the total free energy and its derivative for the system including the solvation medium in order to use the norm-conserving pseudopotentials and projector expansions as follows:

$$\Omega_{\mathrm{tot}} = \Omega_{\mathrm{vac}} + \Omega_{\mathrm{solv}}, \tag{50}$$

$$\Omega_{\mathrm{vac}} = K + E_{\mathrm{xc}} + E_{\mathrm{ec}}^{\mathrm{nl}} + E_{\mathrm{na}} + E_{\mathrm{scc}} + E_{\delta\mathrm{ee}} - TS_e + H_{s,\mathrm{corr}} - TS_s, \tag{51}$$

$$\Omega_{\mathrm{solv}} = \Omega_{\mathrm{solv,el}} + \Omega_{\mathrm{ss,nonel}} + \Omega_{\mathrm{is,nonel}} - TS_i + \Omega_{\mathrm{mc}}, \tag{52}$$

$$E_{\mathrm{xc}} = E_{\mathrm{xc}}\rfloor\rho_{\uparrow} + \rho_{\mathrm{pcc},\uparrow}, \rho_{\downarrow} + \rho_{\mathrm{pcc},\downarrow}\lfloor, \tag{53}$$

$$E_{\mathrm{ec}}^{\mathrm{nl}} = \sum_{\sigma}\sum_{\mathbf{k}}\sum_{i} f_{i\mathbf{k}\sigma}\int d\mathbf{r}\,\psi_{i\mathbf{k}\sigma}^{*}(\mathbf{r})\hat{v}_{\mathrm{nl}}\psi_{i\mathbf{k}\sigma}(\mathbf{r}), \tag{54}$$

$$E_{\mathrm{na}} = \sum_{\sigma}\sum_{\mathbf{k}}\sum_{i} f_{i\mathbf{k}\sigma}\int d\mathbf{r}\,\psi_{i\mathbf{k}\sigma}^{*}(\mathbf{r})\hat{v}_{\mathrm{pr}}\psi_{i\mathbf{k}\sigma}(\mathbf{r}), \tag{55}$$

$$E_{\mathrm{scc}} = \frac{1}{2}{\sum_{\mathbf{R}}}' \sum_{\alpha=1}^{N_{\mathrm{atom}}}\sum_{\beta=1}^{N_{\mathrm{atom}}} \phi_{\alpha\beta}(|\mathbf{R}_{\alpha} - \mathbf{R}_{\beta} - \mathbf{R}|) - 2\pi\sum_{\alpha}\int dr\,\rho_{\mathrm{na},\alpha}(r)\phi_{H,\alpha}(r)r^2, \tag{56}$$

$$E_{\delta\mathrm{ee}} = \frac{1}{2}\int d\mathbf{r}\,\delta\rho_e(\mathbf{r})\,\delta\phi_H(\mathbf{r}), \tag{57}$$

$$\Omega_{\mathrm{solv,el}} = \frac{1}{2}\int d\mathbf{r}[\rho_e(\mathbf{r}) + \rho_c(\mathbf{r})]\phi_{\mathrm{solv}}(\mathbf{r}) + \frac{1}{2}\int d\mathbf{r}[\rho_{-}(\mathbf{r}) + \rho_{+}(\mathbf{r})]\phi(\mathbf{r}). \tag{58}$$

$\hat{v}_{\mathrm{nl}}$ and $\hat{v}_{\mathrm{pr}}$ denote, respectively, the nonlocal pseudopotential and the operator representing a summation of local pseudopotentials and electrostatic potentials from electrons in neutral atoms. ρ_{σ} includes only valence electrons, and $\rho_{\mathrm{pcc},\sigma}$ is the partial core charge with spin σ. $\phi_{\alpha\beta}$ is defined as follows:

$$\phi_{\alpha\beta}(|\mathbf{R}_{\alpha} - \mathbf{R}_{\beta}|) = \frac{Z_{\alpha}Z_{\beta}}{|\mathbf{R}_{\alpha} - \mathbf{R}_{\beta}|} - \int_{\text{all space}} d\mathbf{r}\rho_{\mathrm{na},\alpha}(|\mathbf{r} - \mathbf{R}_{\alpha}|) \times \phi_{H,\beta}(|\mathbf{r} - \mathbf{R}_{\beta}|). \tag{59}$$

$\phi_{H,\alpha}$ is the electrostatic potential of the atomic electron density,

$$\phi_{H,\alpha}(r) = 4\pi\left[\frac{1}{r}\int_{0}^{r} dr'\rho_{\mathrm{na},\alpha}(r')r'^2 + \int_{r}^{\infty} dr'\rho_{\mathrm{na},\alpha}(r')r'\right]. \tag{60}$$

$\delta\rho_e$ is the difference between ρ_e and ρ_{na},

$$\delta\rho_e(\mathbf{r}) = \rho_e(\mathbf{r}) - \rho_{\mathrm{na}}(\mathbf{r}). \tag{61}$$

$\delta\phi_H$ is the electrostatic potential due to $\delta\rho_e$ in the vacuum, and we define it as

$$\delta\phi_H(\mathbf{r}) = \phi_H(\mathbf{r}) - \phi_{H,\mathrm{na}}(\mathbf{r}). \tag{62}$$

ϕ_H is the electrostatic potential obtained by solving the Poisson equation written as follows:

$$\nabla^2\phi_H(\mathbf{r}) = -4\pi\rho_e(\mathbf{r}). \tag{63}$$

$\phi_{H,\mathrm{na}}$ is the summation of the electrostatic potentials caused by electrons in neutral atoms,

$$\phi_{H,\mathrm{na}}(\mathbf{r}) = \sum_{\mathbf{R}}\sum_{\alpha=1}^{N_{\mathrm{atom}}} \phi_{H,\alpha}(|\mathbf{r} - \mathbf{R}_{\alpha} - \mathbf{R}|). \tag{64}$$

ρ_c and ϕ_c are the charge distribution of pseudoatomic cores in the vacuum and its electrostatic potential, and these are written as

$$\rho_c(\mathbf{r}) = -\sum_{\mathbf{R}} \sum_{\alpha=1}^{N_{\text{atom}}} Z_\alpha \delta(\mathbf{r} - \mathbf{R}_\alpha - \mathbf{R}), \tag{65}$$

$$\phi_c(\mathbf{r}) = -\sum_{\mathbf{R}} \sum_{\alpha=1}^{N_{\text{atom}}} \frac{Z_\alpha}{|\mathbf{r} - \mathbf{R}_\alpha - \mathbf{R}|}, \tag{66}$$

where Z_α is the number of valence electrons for each atom. ϕ_{solv} is the solvation contribution to the total electrostatic potential, defined as

$$\phi_{\text{solv}}(\mathbf{r}) = \phi(\mathbf{r}) - \phi_H(\mathbf{r}) - \phi_c(\mathbf{r}). \tag{67}$$

The Kohn–Sham Hamiltonian is rewritten as

$$\hat{H}_\sigma = \hat{H}_{\sigma,\text{vac}} + \phi_{\text{solv}}(\mathbf{r}), \tag{68}$$

$$\hat{H}_{\sigma,\text{vac}} = -\frac{1}{2}\nabla^2 + \delta\phi_H(\mathbf{r}) + v_{\sigma,\text{xc}}(\mathbf{r}) + \hat{v}_{\text{nl}}(\mathbf{r}) + \hat{v}_{\text{pr}}(\mathbf{r}). \tag{69}$$

The analytical derivatives of Eq. (50) are summarized as follows:

$$\nabla_{\mathbf{R}_\alpha}\Omega_{\text{tot}} = -\mathbf{F}_{\text{vac}} - \mathbf{F}_{\text{Pulay}} - \mathbf{F}_{\text{solv}}, \tag{70}$$

$$\mathbf{F}_{\text{vac}} = \mathbf{F}_{\text{ec}}^{\text{nl}} + \mathbf{F}_{\text{na}} + \mathbf{F}_{\text{scc}} + \mathbf{F}_{\delta\text{ee}} + \mathbf{F}_{\text{pcc}}, \tag{71}$$

$$\mathbf{F}_{\text{solv}} = \mathbf{F}_{\text{solv,el}} + \mathbf{F}_{\text{solv,nonel}}, \tag{72}$$

$$\mathbf{F}_{\text{ec}}^{\text{nl}} = -\sum_\sigma \sum_{\mathbf{k}} \sum_i f_{i\mathbf{k}\sigma} \int d\mathbf{r}\, \psi_{i\mathbf{k}\sigma}^*(\mathbf{r})(\nabla_{\mathbf{R}_\alpha}\hat{v}_{\text{nl}})\psi_{i\mathbf{k}\sigma}(\mathbf{r}), \tag{73}$$

$$\mathbf{F}_{\text{na}} = -\sum_\sigma \sum_{\mathbf{k}} \sum_i f_{i\mathbf{k}\sigma} \int d\mathbf{r}\, \psi_{i\mathbf{k}\sigma}^*(\mathbf{r})(\nabla_{\mathbf{R}_\alpha}\hat{v}_{\text{pr}})\psi_{i\mathbf{k}\sigma}(\mathbf{r}), \tag{74}$$

$$\mathbf{F}_{\text{scc}} = -\sum_{\mathbf{R}}{}' \sum_{\beta=1}^{N_{\text{atom}}} \nabla_{\mathbf{R}_\alpha}\phi_{\alpha\beta}(|\mathbf{R}_\alpha - \mathbf{R}_\beta - \mathbf{R}|), \tag{75}$$

$$\mathbf{F}_{\delta\text{ee}} = \int d\mathbf{r}\, \delta\phi_H(\mathbf{r})\nabla_{\mathbf{R}_\alpha}\rho_{\text{na}}(\mathbf{r}), \tag{76}$$

$$\mathbf{F}_{\text{pcc}} = -\sum_\sigma \int d\mathbf{r}\nabla_{\mathbf{R}_\alpha}\rho_{\text{pcc},\sigma}(\mathbf{r})v_{\text{xc},\sigma}(\mathbf{r}), \tag{77}$$

$$\mathbf{F}_{\text{solv,el}} = Z_\alpha \nabla_{\mathbf{R}_\alpha}\phi_{\text{solv}}(\mathbf{R}_\alpha). \tag{78}$$

$\mathbf{F}_{\text{Pulay}}$ and $\mathbf{F}_{\text{solv,nonel}}$ are same as those in Sec. II A.

Figure 4 shows the flowchart for the self-consistent field (SCF) procedure with the solvation medium. The additional computational cost for including solvation in the calculations is due to finding ϕ_{solv} on three-dimensional numerical integration grids. In solving the Poisson equation, we applied an efficient method combining a multigrid technique[92] with a parallel successive over-relaxation method[93] using regular real-space grids. A v-cycle method with a nested iteration technique was used in the multigrid method.[92] ϕ_{solv} on the integration grids were calculated through three-dimensional bicubic interpolations of ϕ_{solv} on the regular real-space grids. The additional computational cost for the solvation calculation was about 7% of the total computational cost.

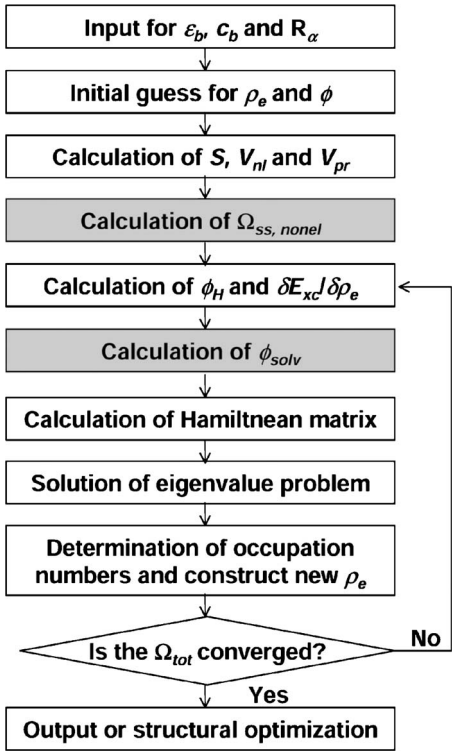

FIG. 4. Flowchart for the SCF procedure. The shaded squares mean additional parts needed for systems including the solvation medium.

C. Details of model and computation

The Pt(111) surface was modeled by three layers of slabs with the theoretically predicted lattice constant of 4.03 Å for RPBE and 4.00 Å for PBE using a bulk crystal model. We found that a slab model with four layers gives a 0.02 eV stronger adsorption energy for water at 1/4 monolayer coverage, but we consider that such a difference does not significantly change conclusions based on calculations in this study. We used rectangular $\sqrt{3}\times 2$ and $\sqrt{3}\times 3$ unit cells. The solution was modeled by combinations of a few explicit water molecules handled by the DFT and the continuum solvation model handled by the MPB. We applied the boundary condition as shown in Fig. 1(b). The Brillouin-zone integrations were performed with $5\times 6\times 1$ grids for the $\sqrt{3}\times 2$ unit cell and $3\times 6\times 1$ grids for the $\sqrt{3}\times 3$ unit cell. The atoms in the bottom layers of the slabs were fixed in position, and the other atoms were relaxed with the criteria of 0.05 eV/Å for the maximum force. The electrode potential on the SHE scale is calculated from the Fermi energy as

$$U = -\frac{\varepsilon_F - \phi_{\text{SHE}}}{e}. \tag{79}$$

ϕ_{SHE} is the thermodynamic work function of the SHE, for which we used theoretically predicted values of –4.43 eV

for RPBE and –4.30 eV for PBE.[62] These values are in the range of experimental values from –4.80 to –4.28 eV.[94,95]

III. RESULTS AND DISCUSSION

A. Potential of zero charge

1. Potential of zero charge from vacuum calculations

The work function of the Pt(111) surface in a vacuum was measured as 5.6–6.4 eV.[96–103] If we use 6.0 eV, which is the middle of the experimental range, the PZC of the Pt(111) surface in a vacuum is calculated as about 1.6 V in the SHE scale by using Eq. (79) with ϕ_{SHE} for RPBE. The PZC of the Pt(111) surface in aqueous solutions is still a controversial issue, and many experimental works using 0.1 N perchloric acid electrolytes suggest that the PZC is at the onset of hydrogen adsorption [i.e., 0.34 V (Ref. 104) and 0.35 V (Ref. 105) on the reversible hydrogen electrode (RHE) scale] or nearby within the double-layer region [i.e., 0.43 V (RHE) (Ref. 106)]. To convert these potentials for 0.1 N acid to the SHE scale, 0.06 V must be subtracted from the RHE potentials. A study using the immersion technique gave a substantially higher value of 0.84 V (RHE).[107] If we use an average PZC of 0.4 V (RHE) based on the three experimental results in Refs. 104–106, the decrease in the PZC by solvation is estimated as 1.2 V. Decreases in the PZC of transition metal surfaces caused by the adsorption of water molecules were also reported in previous experimental and theoretical studies.[108–112] Although the PZC also depends on the *p*H of the solutions,[113] water molecule adsorption seems to be the main influence on the decrease in the PZC.

The mechanism of this phenomenon is not clearly explained yet. Trasatti[114] proposed a phenomenological view that the PZC is influenced by both the orientation of dipole moments of adsorbed solvent molecules and the changes in the metal surface dipole due to contact with solutions. Because of the small adsorption energy for water, the orientation of the water dipoles has been considered to dominate the decrease in the PZC. However, such a simple picture of the mechanism was considered questionable because of the recently discovered evidence that a so-called bilayer of water molecules with an *H*-down structure [see Fig. 5(g)] is more stable than that with an *H*-up structure [see Fig. 5(h)] at the interface between a vacuum and the Pt(111) surface.[115]

In this section, we present the results of the PZC calculated by the various models shown in Figs. 5(a)–5(h) without the continuum solvation model. The model in Fig. 5(a) is the bare Pt(111) surface. The models in Figs. 5(b) and 5(c) are rectangular $\sqrt{3}\times 2$ unit cells with 1/4 and 1/2 monolayer (ML) coverages, respectively, by water molecules. The models in Figs. 5(d)–5(h) are rectangular $\sqrt{3}\times 3$ unit cells with 1/6, 1/3, 1/2, 2/3, and 2/3 ML coverages, respectively. Information about the optimized structures and adsorption free energies is summarized in Table I. The calculated PZC values are plotted as a function of the coverage of water molecules in Fig. 6 and listed in Table I.

Before discussing the PZC results, we comment on the accuracy of our newly developed code for the adsorption energies of water molecules. Our laboratory performed a first

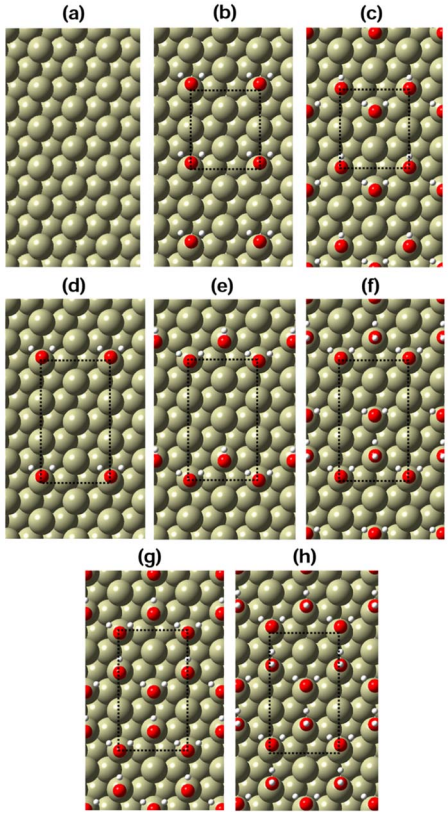

FIG. 5. (Color online) Top views of the models for the PZC calculations. The coverages for water molecules are (a) 0, (b) 1/4, (c) 1/2, (d) 1/6, (e) 1/3, (f) 1/2, (g) 2/3, and (h) 2/3 ML. The dotted lines show translation unit cells. The big, medium, and small spheres show Pt, O, and H atoms, respectively.

principles calculation using plane wave basis sets, ultrasoft pseudopotentials, and the GGA-PW91 functional and obtained an adsorption energy of 0.23 eV per water molecule using a (2×2) translational unit cell to represent 1/4 ML coverage.[15] Using a similar method, Vassilev *et al.*[116] obtained 0.30 eV per water molecule at 1/3 ML using a $(\sqrt{3}\times\sqrt{3})$ translational unit cell. Our results of 0.28 eV for 1/6 ML and 0.21 eV for 1/4 ML using RPBE are close to these previous results. The adsorption energies of water molecules for models g and h were calculated by Vassilev *et al.*,[116] and they got 0.50 eV for model g and 0.46 eV for model h. Our results are 0.35 and 0.33 eV, respectively, and these are slightly lower than the values in the previous study. We also performed calculations by using the PBE functional, which is a simplified version of GGA-PW91,[67] and obtained 0.60 and 0.54 eV, respectively, which are closer to the previous results. We think that PBE gives stronger hydrogen bonds than those given by RPBE. All calculations showed that model g is more stable than model h in the vacuum condition, and these results qualitatively agree with experiment.[115] All free energy changes by adsorptions are positive; therefore, water molecules on the surface are less stable than those in the gas phase.

The adsorption of explicit water molecules with any

TABLE I. Distances l_{AB} (Å), angles a_{ABC} (°), adsorption free energies $\Delta\Omega_{ads}$ (eV), adsorption energies ΔE_{ads} (eV), and PZCs U_{PZC} (V) (SHE) from vacuum calculations. ∥ and ⊥ denote water molecules with the H-O-H plane parallel to the surface and with the H-O-H plane normal to the surface, respectively. Hu denotes the hydrogen atom with a higher z position than that of Hd.

	Structure	$\Delta\Omega_{ads}$ (ΔE_{ads})	U_{PZC}
a			1.53
b	l_{PtO}=2.47, l_{OH}=0.98, a_{HOH}=101.4, a_{PtOH}=91.7	0.28(−0.21)	0.80 (0.40)
c	$l_{PtO,\parallel}$=2.45, $l_{OH,\parallel}$=0.98, $a_{HOH,\parallel}$=103.1, $a_{PtOH,\parallel}$ =103.3, $l_{PtO,\perp}$=3.31, $l_{OHd,\perp}$=0.99, $l_{OHu,\perp}$ =0.98, $a_{HOH,\perp}$=100.8, $a_{PtOHu,\perp}$=167.8	0.18(−0.32)	−0.24 (0.30)
d	l_{PtO}=2.57, l_{OH}=0.98, a_{HOH}=101.1, a_{PtOH}=89.9	0.22(−0.28)	0.87 (0.68)
e	$l_{PtO,\parallel}$=2.36, $l_{OH,\parallel}$=0.99, $a_{HOH,\parallel}$=103.4, $a_{PtOH,\parallel}$ =106.2, $l_{PtO,\perp}$=3.24, $l_{OHd,\perp}$=1.00, $l_{OHu,\perp}$ =0.98, $a_{HOH,\perp}$=101.5, $a_{PtOHu,\perp}$=96.0	0.14(−0.36)	0.12 (0.45)
f	$l_{PtO,\parallel 1}$=2.36, $l_{OH,\parallel 1}$=0.99, $a_{HOH,\parallel 1}$ =103.9, $a_{PtOH,\parallel 1}$=104.2, $l_{PtO,\perp}$=3.45, $l_{OHd,\perp}$ =0.99, $l_{OHu,\perp}$=0.97, $a_{HOH,\perp}$=102.3, $a_{PtOHu,\perp}$ =173.0, $l_{PtO,\parallel 2}$=3.28, $l_{OH,\perp 2}$=0.98, $a_{HOH,\parallel 2}$ =99.6, $a_{PtOH,\parallel 2}$=58.0	0.13(−0.37)	0.09 (0.39)
g	$l_{PtO\parallel}$=2.72, l_{OH}=0.99, $a_{HOH\parallel}$=104.0, $a_{PtOH\parallel}$ =104.3, $l_{PtO,\perp}$=3.25,$l_{OHd,\perp}$=1.00, $l_{OHu,\perp}$ =0.99, $a_{HOH,\perp}$=98.5, $a_{PtOHu,\perp}$=98.6	0.15(−0.35)	0.90 (0.56)
h	$l_{PtO\parallel}$=2.78, $l_{OH,\parallel}$=0.99, $a_{HOH,\parallel}$=105.4, $a_{PtOH,\parallel}$ =98.0, $l_{PtO,\perp}$=3.52, $l_{OHd\perp}$=0.99, $l_{OHu\parallel}$=0.98, $a_{HOH,\perp}$ =100.8, $a_{PtOHu,\perp}$=167.8	0.17(−0.33)	−1.25 (0.25)

coverage lowers the PZC of the Pt(111) surface, as shown in Fig. 6. This trend is similar to the experimentally observed negative shift of the PZC by solvation. However, the amplitude of the shift fluctuates with the coverage and the configuration of water molecules. The reason for this fluctuation is explained by changes in the interfacial dipole moment. As shown in Fig. 7, the amplitudes agree well with the potential drops by net dipole moments in the z direction defined as

$$\Delta\phi_{dip} = -\frac{4\pi d}{S}, \tag{80}$$

$$d = \int d\mathbf{r}[\rho_e(\mathbf{r}) + \rho_c(\mathbf{r})]z. \tag{81}$$

There are two contributions to the net dipole moment. One is the dipole moment due to the orientations of water molecules, and the other is the dipole moment due to charge redistributions caused by adsorptions. In this study, we call the former effect the orientation effect and the later effect the polarization effect. We determined the potential drops $\Delta\phi_{dip,ori}$ due to the orientation effect by calculations of iso-

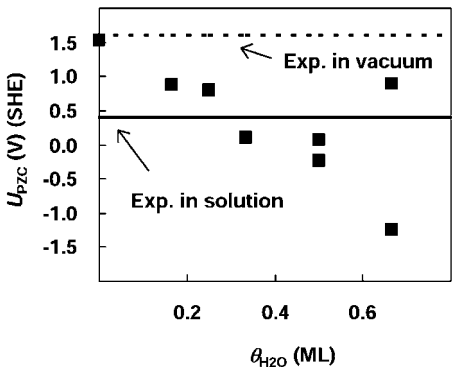

FIG. 6. PZC U_{PZC} (V) (SHE) as a function of the coverage for water molecules and θ_{H2O} (ML) from vacuum calculations. The squares are calculated PZCs. The solid line is the experimentally measured PZC in solutions, and the dotted line is the experimentally measured PZC in the vacuum.

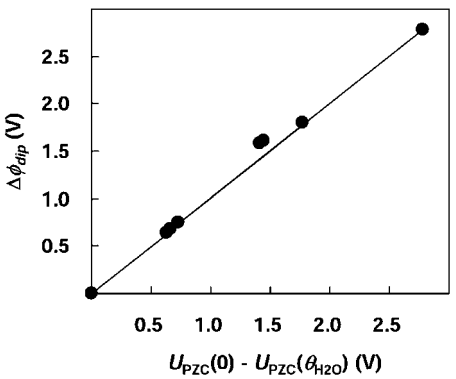

FIG. 7. Potential drop $\Delta\phi_{dip}$ (V) caused by the net dipole moment in the z direction of the system as a function of the change in the PZC by adsorptions of water molecules, $U_{PZC}(\theta_{H2O}) - U_{PZC}(0)$ (V). The circles correspond to calculated data. The solid line is a diagonal line.

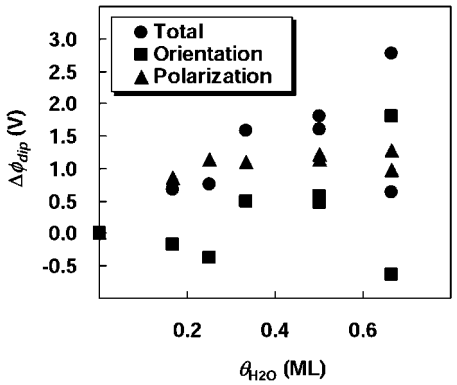

FIG. 8. Potential drops $\Delta\phi_{\mathrm{dip}}$ (V) caused by the total dipole moment, the dipole moment by water orientations, and the dipole moment due to charge redistributions caused by the adsorption as functions of the coverage of water molecules, θ_{H2O} (ML).

lated water adsorbates with the same configurations as those in total systems, and summarized the data in Fig. 8. A quite interesting point is that the potential drops $\Delta\phi_{\mathrm{dip,pol}}$ due to the polarization effect, which were calculated by subtracting $\Delta\phi_{\mathrm{dip,ori}}$ from $\Delta\phi_{\mathrm{dip}}$, do not fluctuate so much. $\Delta\phi_{\mathrm{dip,pol}}$ increases with the increase in the coverage from 0 to 1/4 ML and converges to 1.1 V. The reason for the increase in $\Delta\phi_{\mathrm{dip,pol}}$ in the low coverage region is interpreted as more charge redistributions due to the increase in the number of interactions between the water molecules and the surface. In addition to this interesting behavior, the result consistent with the experimental PZC is obtained by using $\Delta\phi_{\mathrm{dip,pol}}$ as the negative shift of the PZC from that in the vacuum, as shown in Fig. 9. According to this dipole analysis, we expect that the charge redistributions due to the adsorption of water molecules is the main reason for the negative shift of the PZC, and the dipole moment caused by interfacial water orientations shown in these vacuum calculations is canceled out in actual interfaces.

The structure of the charge redistributions caused by water adsorption is defined as

$$\Delta\rho(\mathbf{r}) = \rho_{e,\mathrm{tot}}(\mathbf{r}) - \rho_{e,\mathrm{Pt}}(\mathbf{r}) - \rho_{e,n\mathrm{H_2O}}(\mathbf{r}), \tag{82}$$

where $\rho_{e,\mathrm{tot}}$, $\rho_{e,\mathrm{Pt}}$, and $\rho_{e,n\mathrm{H_2O}}$ are the electron densities in the total system, the system including the Pt surface, and the

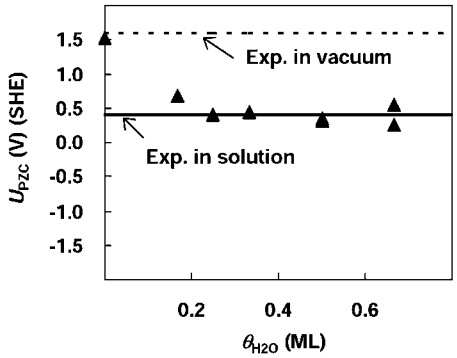

FIG. 9. PZC U_{PZC} (V) (SHE), calculated as $U_{\mathrm{PZC}}(0) - \Delta\phi_{\mathrm{dip,pol}}(\theta_{\mathrm{H2O}})$, as a function of the coverage of water molecules, θ_{H2O} (ML). The solid and dotted lines are the same as those in Fig. 6.

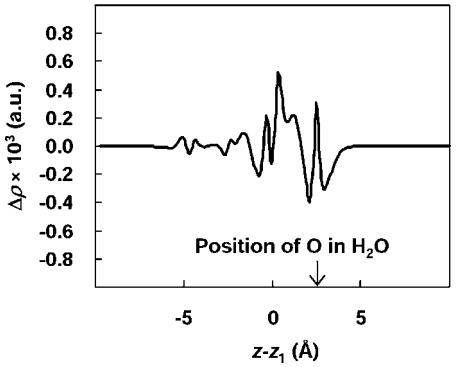

FIG. 10. Charge redistributions caused by the adsorption of water molecules for model d. $\Delta\rho$ is the change in the electron density due to adsorption of water.

system including adsorbates, respectively. In Fig. 10, we show the averaged $\Delta\rho$ within the x-y planes for model d. Figure 10 shows a polarization in the region from the position of the top layer of the slab to the position just above the water molecule. The water molecule is positively charged, and the top layer of slab is negatively charged.

2. Potential of zero charge from solvation calculations

Now, we have two essential questions about the abilities of our continuum solvation model. First, can the continuum solvation model reproduce the polarization effects? Second, can the continuum solvation model cancel the orientation effects? We present similar calculations to those shown in Sec. III A 1 but using the continuum solvation model, in order to answer these questions. Figure 11 shows the calculated PZC as a function of the coverage of explicit water molecules handled by the DFT. The PZC values from Figs. 6 and 9 are also plotted in Fig. 11. The structural data, adsorption free energies, and all PZC values are listed in Table II.

Before the discussion of the PZC, we describe the changes in structures and adsorption free energies due to the

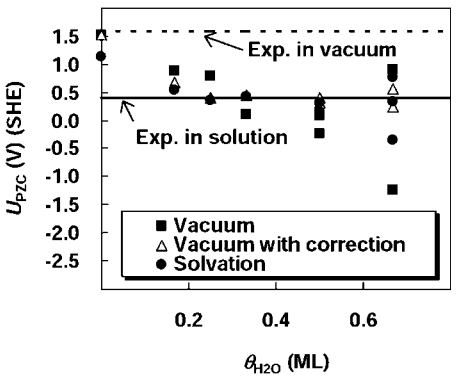

FIG. 11. PZCs U_{PZC} (V) (SHE) calculated from three different methods. The squares denote the PZCs calculated from vacuum calculations, the triangles denote the PZCs calculated from vacuum calculations with the correction to dipole moments caused by water orientations, and the circles denote the PZCs calculated from solvation calculations. The solid and dotted lines are same as those in Fig. 6.

TABLE II. Distances l_{AB} (Å), angles a_{ABC} (°), adsorption free energies $\Delta\Omega_{ads}$ (eV), and PZCs U_{PZC} (V) (SHE) from solvation calculations.

	Structure	$\Delta\Omega_{ads}$	U_{PZC}
a			1.13
b	$l_{PtO}=2.45$, $l_{OH}=0.98$, $a_{HOH}=101.9$, $a_{PtOH}=100.3$	0.07	0.36
c	$l_{PtO,\parallel}=2.46$, $l_{OH,\parallel}=0.99$, $a_{HOH,\parallel}=105.6$, $a_{PtOH,\parallel}=103.2$, $l_{PtHd,\perp}=3.25$,$l_{OHd,\perp}=0.99$, $l_{OHu,\perp}=0.98$, $a_{HOH,\perp}=102.5$, $a_{PtOHu\perp,}=103.9$	0.08	0.15
d	$l_{PtO}=2.52$, $l_{OH}=0.98$, $a_{HOH}=102.0$, $a_{PtOH}=96.0$	−0.05	0.54
e	$l_{PtO,\parallel}=2.40$, $l_{OH,\parallel}=1.00$, $a_{HOH,\parallel}=104.0$, $a_{PtOH,\parallel}=106.4$, $l_{PtO,\perp}=3.30$,$l_{OHd,\perp}=0.99$, $l_{OHu,\perp}=0.98$, $a_{HOH,\perp}=103.2$, $a_{PtOHu,\perp}=144.2$	−0.04	0.42
f	$l_{PtO,\parallel1}=2.37$, $l_{OH,\parallel1}=0.99$, $a_{HOH,\parallel1}=104.3$, $a_{PtOH,\parallel1}=105.0$, $l_{PtO,\perp}=3.35$, $l_{OHd,\perp}=0.99$, $l_{OHu,\perp}=0.98$, $a_{HOH,\perp}=102.7$,$a_{PtOHu,\perp}=142.6$, $l_{PtO,\parallel2}=3.31$, $l_{OH,\parallel2}=0.98$, $a_{HOH,\parallel2}=100.5$	−0.02	0.30
g	$l_{PtO,\parallel}=2.54$, $l_{OH,\parallel}=0.99$, $a_{HOH,\parallel}=103.2$, $a_{PtOH,\parallel}=104.6$, $l_{PtO,\perp}=3.20$,$l_{OHd,\perp}=1.00$, $l_{OHu,\perp}=0.99$, $a_{HOH,\perp}=98.8$, $a_{PtOHu,\perp}=97.3$	0.04	0.34
h	$l_{PtO,\parallel}=2.75$, $l_{OH,\parallel}=0.99$, $a_{HOH,\parallel}=104.5$, $a_{PtOH,\parallel}=97.9$, $l_{PtO,\perp}=3.48$,$l_{OHd,\perp}=1.00$, $l_{OHu,\perp}=0.99$, $a_{HOH,\perp}=102.6$, $a_{PtOHu,\perp}=176.9$	0.02	−0.35
h′	$l_{PtO,\parallel}=3.61$, $l_{OH,\parallel}=0.99$, $a_{HOH,\parallel}=104.6$, $a_{PtOH,\parallel}=84.5$, $l_{PtO,\perp}=3.63$,$l_{OHd,\perp}=1.00$, $l_{OHu,\perp}=0.98$, $a_{HOH,\perp}=104.5$, $a_{PtOHu,\perp}=174.0$	0.04	0.74

solvation medium. The overall structural changes caused by the solvation medium are relatively small except in the case of model h. In this case, we found an additional local minimum structure, which we call model h′. Adding the solvation medium decreases the adsorption free energies by an average of 0.22 eV and gives closer values to 0 eV. The fluctuations in the adsorption free energies are relatively small. The adsorption of a water molecule in the solvation medium corresponds to the exchange of a water molecule in the solution for an interfacial water molecule. When these two water molecules are in equilibrium, the free energy change must be zero. Therefore, we consider that results of adsorption free energies in Table II are consistent. The small fluctuations among the different structures in the hydrogen bonding network can be explained with two reasons. First, the strength of the hydrogen bonds among water molecules is relatively small. For example, the strength of the hydrogen bonds in water dimers is around 0.1 eV.[62] Second, in the calculation of the adsorption free energies, the contributions from the hydrogen bonding network in the solution and at the interface cancel out. One thing we have to mention is that the effects of the hydrogen bonding network between interfacial water molecules and other adsorbates, such as OH(ads) or HO_2(ads), are not negligibly small. The specific interactions between H in H_2O(ads) and O in OH(ads) or O in H_2O(ads) and H in HO_2(ads) give a strong influence on the calculated redox potentials forming these adsorbates by 0.2–0.5 V.[62]

The continuum solvation model without any explicit water molecules lowers the PZC by 0.4 V from the value of the bare Pt(111) surface in the vacuum. This result qualitatively agrees with the experimentally observed negative shift of the PZC, but the amplitude of the shift in this study is smaller. The reason for the qualitative agreement and the quantitative disagreement is shown in the following analysis of charge distributions: A transformation of Eq. (44) using variables from Ref. 64 gives a useful interpretation that adding the continuum solvation medium corresponds to replacing the total charge density by an effective charge density ρ_ε in the vacuum,

$$\rho_\varepsilon(\mathbf{r}) = \frac{\rho_e(\mathbf{r}) + \rho_c(\mathbf{r}) + \rho_+(\mathbf{r}) + \rho_-(\mathbf{r})}{\sqrt{\varepsilon(\mathbf{r})}} - \frac{1}{4\pi}\nabla^2\sqrt{\varepsilon(\mathbf{r})}\phi(\mathbf{r}). \tag{83}$$

Now, we can visualize the effect of the solvation medium as the difference of charge densities defined as

$$\Delta\rho_\varepsilon(\mathbf{r}) = \rho_\varepsilon(\mathbf{r}) - \rho(\mathbf{r}), \tag{84}$$

where ρ is the total charge density obtained by the SCF calculation of the Pt(111) surface in the vacuum with the same atomic positions as those from the solvation calculation. $\Delta\rho_\varepsilon$ and $\Delta\rho$ in Sec. III A 1 are shown in Fig. 12. $\Delta\rho_\varepsilon$ has a clear polarization, and the position of the polarization in $\Delta\rho_\varepsilon$ is close to that in $\Delta\rho$. We calculated the potential drop due to $\Delta\rho_\varepsilon$ as 0.38 V, which agrees well with the theoretically obtained amplitude of the negative shift of the PZC. However, $\Delta\rho$ has a more complicated shape with a bigger polarization than that of $\Delta\rho_\varepsilon$. From this analysis, the answer

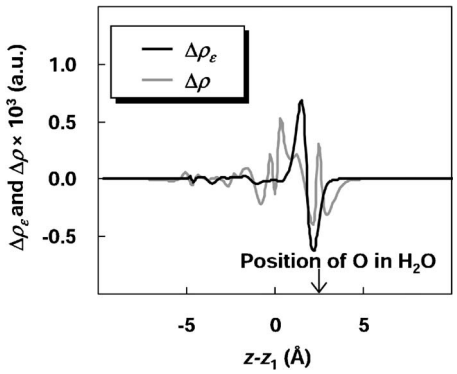

FIG. 12. Charge redistributions $\Delta\rho_\varepsilon$ and $\Delta\rho$ caused by the solvation medium and the adsorption of explicit water molecules for model d.

to the first question is that our continuum solvation model can qualitatively represent polarizations caused by adsorptions, but the potential drop due to the polarization caused by the solvation medium quantitatively disagrees with that caused by the adsorption of explicit water molecules.

We obtained a mean absolute difference of 0.09 V between the results of the solvation calculations and vacuum calculations using the correction to orientation effects as described in Sec. III A 1 in all cases but models h and h′, for which we obtained two quite different PZCs: −0.35 V (SHE) for model h and 0.74 V (SHE) for model h′. Although both values are far from the PZC of 0.25 V (SHE) for model h given from the vacuum calculation with the correction to orientation effects, these are closer than the result of −1.25 V (SHE) given from the vacuum calculation without any correction. Therefore, we can say that the solvation medium partially canceled the effects of water orientations on the PZC. A detailed analysis of dipole moments showed that such a cancellation is the result of a corporative effect by relaxations of atomic positions and $\Delta\rho_\varepsilon$ defined in Eq. (84). As an example, we show results of the dipole analysis for model d in Table III. The solvation medium changed the previously described three dipole moments caused by the orientation effect, the polarization effect, and the effect of $\Delta\rho_\varepsilon$. We denote the potential drops due to changes in these three dipole moments as $\Delta\Delta\phi_{\mathrm{dip,ori}}$, $\Delta\Delta\phi_{\mathrm{dip,pol}}$, and $\Delta\phi_\varepsilon$. A slight change in the Pt-O-H degree from 89.9° to 96.0° gives a $\Delta\Delta\phi_{\mathrm{dip,ori}}$ of 0.47 V. $\Delta\Delta\phi_{\mathrm{dip,pol}}$ due to the relatively small structural change. The potential drop $\Delta\phi_\varepsilon$ due to $\Delta\rho_\varepsilon$ is −0.17 V. The change in the net potential drop $\Delta\Delta\phi_{\mathrm{dip}}$ by the solvation medium becomes 0.30 V, which is in the direction to cancel $\Delta\phi_{\mathrm{dip,ori}}$ of −0.18 V from the vacuum calculation.

TABLE III. Potential drops (V) due to changes in dipole moments caused by the solvation medium. All symbols in this table are defined in the text.

	$\Delta\phi_{\mathrm{dip\ ori}}$ in vacuum	$\Delta\Delta\phi_{\mathrm{dip\ ori}}$	$\Delta\Delta\phi_{\mathrm{dip\ pol}}$	$\Delta\phi_\varepsilon$	$\Delta\Delta\phi_{\mathrm{dip}}$
Potential drop (V)	−0.18	0.47	0.01	−0.17	0.30

The reason for quite different behaviors in the PZC for models h and h′ are not clearly explained yet. Further studies including more explicit water molecules and dynamics of interfacial water molecules might help to answer to the question about these specific results.

B. Poisoning of active sites for oxygen-reduction reaction by water molecules

The big overpotential for the four-electron reduction of an oxygen molecule to water molecules,

$$O_2(g) + 4H^+(aq) + 4e^- \rightarrow 2H_2O(aq), \tag{85}$$

on Pt or Pt alloy catalysts is one of the most serious problems in fuel cell technologies. The onset potential of the ORR is around 0.9–1.0 V on the Pt(111) surface in acid solutions; therefore, the overpotential of 0.2–0.3 V is necessary to activate the ORR.[117] An enormous number of studies including both experimental and theoretical ones have been performed to elucidate reasons for such a big overpotential, as well as to gain a fundamental understanding of the mechanism of the ORR. The reaction pathway of the ORR is still a controversial issue, but it is commonly accepted that the first step of the ORR is the adsorption of the oxygen molecule:[6,117,118]

$$O_2(g) \rightarrow O_2(ads). \tag{86}$$

Furthermore, OH(ads) has been considered as the poisoning adsorbate for the adsorption step.[15,17,19,117,119,120] However, a question about possibilities of other poisoning adsorbates remains because several previous studies showed that improvements in overpotentials were less than those expected from observed apparent decreases in OH(ads). For example, Shao *et al.*[121] developed platinum monolayer oxygen-reduction electrocatalysts with Co-Pd core-shell nanoparticle support and obtained the improvement of only 0.02 V in the overpotential in spite of 0.1 V shift of the onset potential for the water oxidation reaction in a 0.1*M* $HClO_4$ solution. Another example is in the study by Teliska *et al.*,[122] who found that the overpotential is decreased by only 0.05 V in spite of the positive shift of 0.1 V for the onset potential of the water oxidation reaction by increasing the concentration of the trifluoromethanesulfonic acid solution from 1*M* to 6*M*. Although the anion is another possible poisoning adsorbate for the ORR, there has been a big question of whether interfacial water molecules block active sites or not. Previous DFT calculations showed adsorption energies of 0.1–0.7 eV for O_2(ads) [21,123,124] and 0.2–0.3 eV for a water molecule (see Sec. III A) for low coverage conditions. In addition to these overlapping adsorption energies, surface charging may stabilize interfacial water molecules more because of the bigger dipole moment or enhanced lone-pair donation from H_2O to the positively charged metal atom. Therefore, we cannot deny the possibility of surface blocking by water molecules. Unfortunately, we do not have any experimental or theoretical evidence that directly shows the poisoning of active sites by water molecules. Recently, Heaton and Friesen[125] discovered that the slope of the surface stress, which is related to the orientations of water molecules, becomes maximal at the

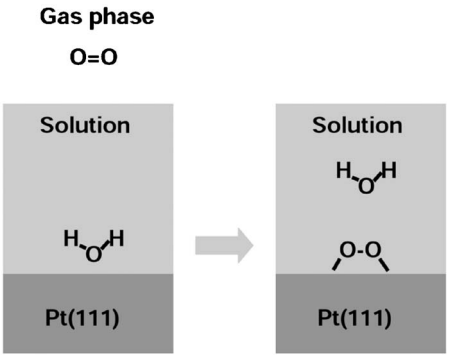

FIG. 13. Schematic of the model for the adsorption of the oxygen molecule on the surface in the solution.

onset potential of the ORR and considered that strongly adsorbed water molecules on the positively charged surface might block the adsorption of oxygen molecules. Although such a correlation gives a new insight into the origin of the big overpotential of ORR, the arguments of Heaton and Friesen[125] using water orientations and interfacial dipole moments were disconnected.

In this section, we present the results of calculations exploring the potential dependencies of free energy changes for reaction (86) on the Pt(111) surface when in a solution. We applied the simple model shown in Fig. 13. In this model, an oxygen molecule in the gas phase replaces an explicit water molecule and forms a bigger cavity at the interface between the surface and the solvation medium, and the desorbed explicit water molecule goes to the solution phase. The free energy of the system before the adsorption was calculated as a summation of the free energies for an isolated O_2 in gas phase and $H_2O/Pt(111)$ in the solvation medium. The free energy of the system after the adsorption was calculated as a summation of the free energies for an isolated H_2O in the solvation medium and $O_2/Pt(111)$ in the solvation medium. The top views of interfacial structures for $H_2O/Pt(111)$ and $O_2/Pt(111)$ are shown in Figs. 14(a) and 14(b). The electrode potential was controlled by adding or removing electrons to or from the systems. In the case of the calculation with RPBE, the excess electron numbers were $-0.10e$, $0.00e$, $0.10e$, $0.20e$, and $0.40e$ for the system before the adsorption

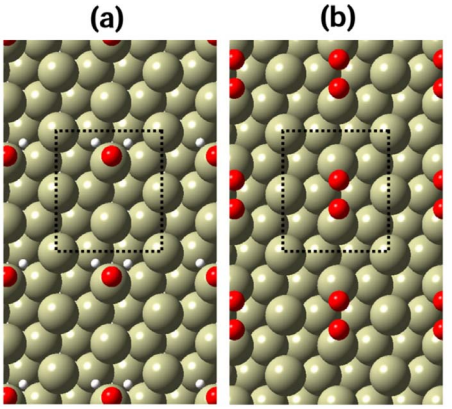

FIG. 14. (Color online) Top view of the surface (a) before and (b) after the adsorption of the oxygen molecule.

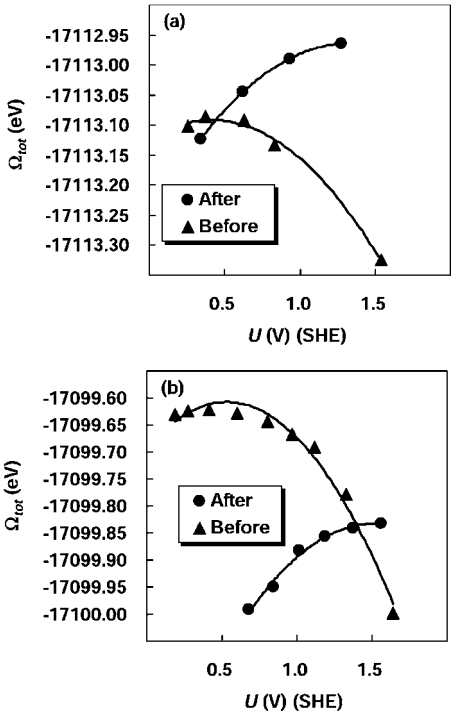

FIG. 15. Total free energies Ω_{tot} (eV) before and after the adsorption of the oxygen molecule as functions of the electrode potential U (V) (SHE). (a) Results by RPBE and (b) results by PBE. The triangles and circles are for systems before and after the adsorption, respectively. The solid lines are free energy curves fitted to the calculated data using least square fittings with quadratic functions.

and $0.00e$, $0.10e$, $0.20e$, and $0.30e$ for the system after the adsorption. In the case of the calculation with PBE, the excess electron numbers were $-0.10e$, $-0.05e$, $0.00e$, $0.05e$, $0.10e$, $0.15e$, $0.20e$, $0.25e$, and $0.35e$ for the system before the adsorption and $0.00e$, $0.05e$, $0.10e$, $0.15e$, $0.20e$, and $0.25e$ for the system after the adsorption. The results of the free energies calculated before and after the adsorption are shown in Figs. 15(a) and 15(b). The free energy change due to the adsorption, which was calculated by quadratic interpolations to the free energy curves, is shown in Fig. 16.

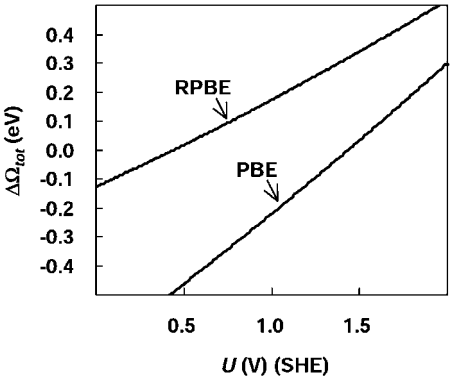

FIG. 16. Free energy changes $\Delta\Omega_{tot}$ (eV) caused by the adsorption of oxygen molecule as a function of electrode potential U (V) (SHE).

TABLE IV. Adsorption energies and magnetic moments of an oxygen molecule, $\Delta E_{\mathrm{ads,O2}}$ (eV) and M_{O2} (μ_B), adsorption energies of an atomic oxygen, $\Delta E_{\mathrm{ads,O}}$ (eV), and binding energies of PtO dimers, $\Delta E_{b,\mathrm{PtO}}$ (eV). The experimental data show the adsorption enthalpy or the dissociation energy.

	$E_{\mathrm{ads,O2}}$	$M_{\mathrm{ads,O2}}$	$E_{\mathrm{ads,O}}$	$E_{b,\mathrm{PtO}}$
This work	−0.36 (RPBE),−0.80 (PBE)	0.75 (RPBE), 0.70 (PBE)	−3.43 (RPBE),−3.95 (PBE)	−3.80 (RPBE),−4.11 (PBE)
Previous calc.	−0.10 (RPBE),[a]−0.72 (PW91)[a]	0.40 (PW91)[a]	−3.27 (RPBE),[b]−3.87 (PBE)[b]	−4.72 (PW91)[c]
Expt.			−3.41 ± 0.33 [d]	−3.82 [e]

[a]Reference 124.
[b]Reference 126.
[c]Reference 127.
[d]Adsorption enthalpies at $\theta_0=1/4$ ML calculated from the data in Refs. 128 and 129.
[e]Dissociation energy in Ref. 130.

Before the discussion of the free energy change in the solution, we mention the accuracy of our newly developed code for the adsorption energies and bond strengths for oxygen atoms or oxygen molecules on surfaces and in dimers in the vacuum condition. The results of these preliminary calculations are summarized in Table IV. Our theory predicts the change in the internal energy due to reaction (86) as 0.36 eV for RPBE and 0.80 eV for PBE. Both results can be interpreted as paramagnetic O_2^- "superoxo" with the magnetic moment of $0.75\mu_B$ for RPBE and $0.70\mu_B$ for PBE. Our calculated adsorption energy using PBE is close to the result of 0.72 eV by Eichler and Hafner[123] using plane wave basis sets, ultrasoft pseudopotentials, and GGA-PW91 for the $(\sqrt{3}\times 2)$ translational unit cell. Our calculated adsorption energy using RPBE is bigger by 0.26 eV than the result by Šlijivančanin and Hammer[124] using plane wave basis sets, ultrasoft pseudopotentials, and GGA-RPBE for the $(3\times\sqrt{7})$ translational unit cell. Our magnetic moment is bigger than $0.4\mu_B$ in the study by Eichler and Hafner.[123] Our theory gives the change in the internal energies due to a following adsorption reaction,

$$\mathrm{O(g)} \rightarrow \mathrm{O(ads)}, \tag{87}$$

as 3.43 eV for RPBE and 3.95 eV for PBE. In this calculation, we used the total energies of atomic oxygen on the fcc hollow site for calculations of adsorption energies. Both results show the atomic oxygen on the surface is nonmagnetic. Ford *et al.*[126] showed that the adsorption energy on Pt(111) with a (2×2) translational unit cell is 3.27 eV for RPBE and 3.87 eV for PBE by using plane wave basis sets and ultrasoft pseudopotentials. Our method gives the bond strength of the PtO dimers in the triplet state as 3.75 eV for PRBE and 4.11 eV for PBE. A previous theoretical method using plane wave basis sets and norm-conserving pseudopotentials with GGA-PW91 predicted a bigger bond strength of 4.72 eV.[127] The mean absolute difference in adsorption energies between our results and previous theoretical results is 0.14 eV. All of the calculations show that RPBE gives smaller adsorption energies than those by PBE. Unfortunately, we could not find reliable experimental data for the adsorption energy for O_2(ads). Experimental measurements suggest that the adsorption enthalpy of reaction (87) with the low coverage limit is 4.34 eV with an error bar of 0.33 eV, and it decreases to 3.21 eV with the increase in the surface coverage of up to 0.65 ML.[128,129] Our theoretical estimates for the thermal corrections to the calculated internal energies give adsorption enthalpies of 3.38 eV for RPBE and 3.89 eV for PBE. Our result by using RPBE is very close to the experimental values of 3.41 eV for 1/4 ML coverage.[128,129] The dissociation enthalpy of 3.73 eV, including the thermal corrections calculated using RPBE for the PtO dimers, is again very close to the experimental result of 3.82 eV.[130] Accordingly, these results and previously demonstrated results for redox potentials of the HOR and the ORR on the Pt(111) surface[62] show that our method using the RPBE functional gives results consistent with experiments for interactions between platinum and adsorbates including oxygen atoms.

The free energy changes due to the adsorption become zero at 0.44 V (SHE) for RPBE and 1.43 V (SHE) for PBE (see Fig. 16). The slopes of these curves are 0.30 eV/V for RPBE and 0.47 eV/V for PBE. Both results show that increasing the electrode potential causes the destabilization of O_2(ads); however, the intersecting points are different by almost 1 V. Such a big difference is caused by the difference between the predicted adsorption energies for O_2(ads). PBE gives the bigger adsorption energy by 0.44 eV than that given from RPBE. We can easily estimate the needed voltage for the further destabilization of O_2(ads) by 0.44 eV as 0.94 V from the slope of 0.47 eV/V for PBE. We calculated the surface coverage of O_2(ads) by using a simple Langmuir adsorption isotherm,

$$\theta_{\mathrm{O_2}} = \frac{e^{-\Delta\Omega_{\mathrm{tot}}/k_BT}}{1+e^{-\Delta\Omega_{\mathrm{tot}}/k_BT}}. \tag{88}$$

Figure 17 shows the results. The result by PBE suggests that there is no blocking by interfacial water molecules in the important potential range of 0.8–1.2 V (SHE) for the ORR; however, the result by RPBE shows a significant decrease in $\theta_{\mathrm{O_2}}$ in this potential range. We consider that the result by RPBE is more reliable because all theoretical results for the adsorption enthalpy of O(ads), the bond strength of the PtO dimers, and the four surface redox potentials for the HOR and the ORR on the Pt(111) surface demonstrated in a previous study[62] and the original work of RPBE for adsorption energies of O(ads), CO(ads) and NO(ads) on Ni, Rh, and Pd surfaces[66] showed that RPBE gives more accurate interac-

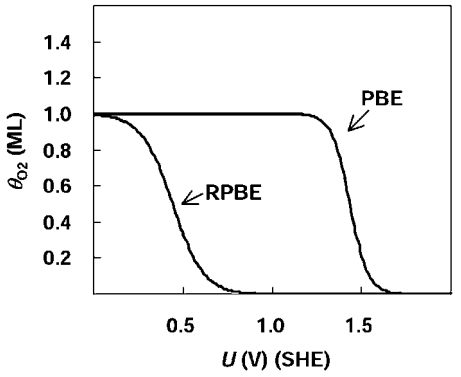

FIG. 17. Coverage of the adsorbed oxygen molecule, θ_{O2} (ML), as a function of electrode potential U (V) (SHE).

tions between adsorbates and transition metal surfaces. Therefore, we consider that there is the possibility of surface blocking by interfacial water molecules. However, we also emphasize that the result is highly sensitive to the adsorption energies of O_2(ads) and interfacial water molecules. In addition to the uncertainties in adsorption energies, surface oxides, such as OH(ads) or O(ads), may have significant effects on the stabilities of O_2(ads) and water molecules. Therefore, we consider that further theoretical and experimental studies including more accurate descriptions of adsorption energies and interactions among adsorbates including surface oxides are necessary to clarify the possibility of surface blocking by interfacial water molecules.

IV. CONCLUDING REMARKS

We have developed a theoretical method for electronic structure calculations for interfaces between liquid solutions and metal surfaces. This method is a combination of a slab model handled by the DFT and a continuum solvation model handled by the MPB through a smooth dielectric function. The free energy formula including cavitation, dispersion, and repulsion free energies and their derivatives with atomic positions were presented. This model has been implemented into a newly developed code using LCPAOs, norm-conserving pseudopotentials, and projector expansion techniques. We applied this methodology to two different topics. One is the PZC of the Pt(111) surface, and the other is the poisoning of active sites for the ORR by interfacial water molecules. The results of the former topic are summarized as follows:

(i) The adsorption of water molecules with a surface coverage of 1/6–2/3 ML lowers the PZC of Pt(111) in the vacuum condition. This trend is similar to the experimentally observed negative shift of the PZC due to immersion of the Pt(111) surface into solutions. However, the calculated PZC fluctuates with change in the coverage and the configuration of water molecules.

(ii) The amplitude of the shift in the PZC by the adsorption of water molecules in the vacuum well agrees with the potential drop due to the dipole moment caused by the water molecules. The detailed dipole analysis showed that the main influence on the fluctuations in PZC is the dipole moment caused by water orientations. Furthermore, the correction to cancel the water orientation effects from the calculated PZC gives a result consistent with the experimental PZC of 0.40 V (SHE). Therefore, we consider that the negative shift of the PZC by solvation is mainly due to the charge redistributions caused by the adsorption.

(iii) Our continuum solvation model qualitatively represents the charge redistributions caused by the adsorption of water molecules; however, the amplitude of the negative shift of the PZC was less by 0.8 V than the experimentally observed one.

(iv) The solvation medium partially canceled the fluctuations in the PZC due to orientations of water molecules shown in the vacuum calculations. Such a cancellation is caused by changes in the atomic positions and charge redistributions by the solvation medium.

The results of the latter topic are summarized as follows:

(i) The results using the RPBE and PBE functionals showed that the increase in the electrode potential destabilizes O_2(ads) with the slopes for free energy changes of 0.30 eV/V for RPBE and 0.47 eV/V for PBE. The intersections where the free energy of O_2(ads) agrees with that of the adsorbed water molecule are 0.44 V (SHE) for RPBE and 1.43 V (SHE) for PBE. This big difference in the intersecting point is caused by the stronger adsorption energy of O_2(ads) given by PBE than that given by RPBE.

(ii) The theory using RPBE, which gives results consistent with experiments, shows a significant decrease in the coverage for O_2(ads) in the important potential region of $U > 0.8$ V (SHE) for the ORR. This suggests the possibility of the poisoning of active sites for the ORR by interfacial water molecules. However, our theory also shows that results are highly sensitive to the calculated bond strengths. We need further theoretical and experimental investigations including more accurate evaluations of adsorption energies for O_2(ads) and water molecules and interactions from surface oxides to these adsorbates in order to clarify the possibility of the surface blocking by interfacial water molecules.

Finally, we believe that our new theoretical method will find many applications in the field of electrocatalysis.

ACKNOWLEDGMENTS

This work was supported by Toyota Central R&D Laboratories, Inc. and by a Multi-University Research-Initiative (MURI) Grant No. DAAD19-03-1-0169 from the U.S. Army Research Office to Case Western Reserve University.

[1] P. Hohenberg and W. Kohn, Phys. Rev. **136**, B864 (1964).
[2] W. Kohn and L. J. Sham, Phys. Rev. **140**, A1133 (1965).
[3] A. B. Anderson and T. V. Albu, J. Am. Chem. Soc. **121**, 11855 (1999).
[4] J. K. Nørskov, T. Bligaard, A. Logadottir, J. R. Kitchin, J. G. Chen, S. Pandelov, and U. Stimming, J. Electrochem. Soc. **152**, J23 (2005).
[5] J. K. Nørskov, J. Rossmeisl, A. Logadottir, L. Lindqvist, J. R. Kitchin, T. Bligaard, and H. Jónsson, J. Phys. Chem. B **108**, 17886 (2004).
[6] A. B. Anderson and T. V. Albu, J. Electrochem. Soc. **147**, 4229 (2000).
[7] A. B. Anderson, N. M. Neshev, R. A. Sidik, and P. Shiller, Electrochim. Acta **47**, 2999 (2002).
[8] A. B. Anderson and N. M. Neshev, J. Electrochem. Soc. **149**, E383 (2002).
[9] R. A. Sidik and A. B. Anderson, J. Electroanal. Chem. **528**, 69 (2002).
[10] A. B. Anderson, Electrochim. Acta **47**, 3759 (2002).
[11] A. B. Anderson, R. A. Sidik, J. Narayanasamy, and P. Shiller, J. Phys. Chem. B **107**, 4618 (2003).
[12] J. Narayanasamy and A. B. Anderson, J. Phys. Chem. B **107**, 6898 (2003).
[13] J. Narayanasamy and A. B. Anderson, J. Electroanal. Chem. **554-555**, 35 (2003).
[14] A. B. Anderson, Electrochim. Acta **48**, 3743 (2003).
[15] J. Roques and A. B. Anderson, J. Electrochem. Soc. **151**, E85 (2004).
[16] A. B. Anderson and R. A. Sidik, J. Phys. Chem. B **108**, 5031 (2004).
[17] J. Roques and A. B. Anderson, J. Electrochem. Soc. **151**, E340 (2004).
[18] Y. Cai and A. B. Anderson, J. Phys. Chem. B **109**, 7557 (2005).
[19] J. Roques, A. B. Anderson, V. S. Murthi, and S. Mukerjee, J. Electrochem. Soc. **152**, E193 (2005).
[20] H. Schweiger, E. Vayner, and A. B. Anderson, Electrochem. Solid-State Lett. **8**, A585 (2005).
[21] J. Roques and A. B. Anderson, J. Fuel Cell Sci. Technol. **2**, 86 (2005).
[22] R. A. Sidik, A. B. Anderson, N. P. Subramanian, S. P. Kumaraguru, and B. N. Popov, J. Phys. Chem. B **110**, 1787 (2006).
[23] J. Roques and A. B. Anderson, Surf. Sci. **581**, 105 (2005).
[24] R. A. Sidik, A. B. Anderson, N. P. Subramanian, S. P. Kumaraguru, and B. N. Popov, J. Phys. Chem. B **110**, 1787 (2006).
[25] R. A. Sidik and A. B. Anderson, J. Phys. Chem. B **110**, 936 (2006).
[26] E. Vayner and A. B. Anderson, J. Phys. Chem. C **111**, 9330 (2007).
[27] E. Vayner, R. A. Sidik, and A. B. Anderson, J. Phys. Chem. C **111**, 10508 (2007).
[28] E. Vayner, H. Schweiger, and A. B. Anderson, J. Electroanal. Chem. **607**, 90 (2007).
[29] V. Stamenkovic, B. S. Mun, K. J. J. Mayrhofer, P. N. Ross, N. M. Markovic, J. Rossmeisl, J. Greeley, and J. K. Nørskov, Angew. Chem., Int. Ed. **45**, 2897 (2006).
[30] J. Greeley, T. F. Jaramillo, J. Bonde, I. B. Chorkendorff, and J. K. Nørskov, Nat. Mater. **5**, 909 (2006).
[31] J. Greeley and J. K. Nørskov, Surf. Sci. **601**, 1590 (2007).
[32] G. S. Karlberg, T. F. Jaramillo, E. Skúlason, J. Rossmeisl, T. Bligaard, and J. K. Nørskov, Phys. Rev. Lett. **99**, 126101 (2007).
[33] J. Rossmeisl, J. K. Nørskov, C. D. Taylor, M. J. Janik, and M. Neurock, J. Phys. Chem. B **110**, 21833 (2006).
[34] M. F. Toney, J. N. Howard, J. Richer, G. L. Borges, J. G. Gordon, O. R. Melroy, D. G. Wiesler, D. Yee, and L. B. Sorensen, Nature (London) **368**, 444 (1994).
[35] J. O'M Bockris and S. U. M. Khan, *Surface Electrochemistry: A Molecular Level Approach* (Plenum, New York, 1993), Chap. 2, p. 59.
[36] R. W. Zwanzig, J. Chem. Phys. **22**, 1420 (1954).
[37] W. L. Jorgensen and C. Ravimohan, J. Chem. Phys. **83**, 3050 (1985).
[38] A. Jean-Charles, A. Nicholls, K. Sharp, B. Honig, A. Tempczyk, T. F. Hendrickson, and W. C. Still, J. Am. Chem. Soc. **113**, 1454 (1991).
[39] V. Mohan, M. E. Davis, J. A. McCammon, and B. M. Pettitt, J. Phys. Chem. **96**, 6428 (1992).
[40] D. Riccardi, P. Schaefer, Y. Yang, H. Yu, N. Ghosh, X. Prat-Resina, P. König, G. Li, D. Xu, H. Guo, M. Elstner, and Q. Cui, J. Phys. Chem. B **110**, 6458 (2006).
[41] M. R. Reddy, U. C. Singh, and M. D. Erion, J. Am. Chem. Soc. **126**, 6224 (2004).
[42] J. Tomasi and M. Persico, Chem. Rev. (Washington, D.C.) **94**, 2027 (1994).
[43] S. Miertš, E. Scrocco, and J. Tomasi, Chem. Phys. **55**, 117 (1981).
[44] M. Cossi, V. Barone, R. Cammi, and J. Tomasi, Chem. Phys. Lett. **255**, 327 (1996).
[45] A. Klamt and G. Schüürmann, J. Chem. Soc., Perkin Trans. 2 **2**, 799 (1993).
[46] C. J. Cramer and D. G. Truhlar, J. Am. Chem. Soc. **113**, 8305 (1991).
[47] C. P. Kelly, C. J. Cramer, and D. G. Truhlar, J. Chem. Theory Comput. **1**, 1133 (2005).
[48] A. Y. Lozovoi, A. Alavi, J. Kohanoff, and R. M. Lynden-Bell, J. Chem. Phys. **115**, 1661 (2001).
[49] A. Y. Lozovoi and A. Alavi, Phys. Rev. B **68**, 245416 (2003).
[50] D. Cao, G.-Q. Lu, A. Wieckowski, S. A. Wasileski, and M. Neurock, J. Phys. Chem. B **109**, 11622 (2005).
[51] C. D. Taylor, S. A. Wasileski, J.-S. Filhol, and M. Neurock, Phys. Rev. B **73**, 165402 (2006).
[52] J. Rossmeisl, J. K. Nørskov, C. D. Taylor, M. J. Janik, and M. Neurock, J. Phys. Chem. B **110**, 21833 (2006).
[53] J.-S. Filhol and M. Neurock, Angew. Chem., Int. Ed. **45**, 402 (2006).
[54] C. D. Taylor, R. G. Kelly, and M. Neurock, J. Electrochem. Soc. **153**, E207 (2006).
[55] O. Sugino, I. Hamada, M. Otani, Y. Morikawa, T. Ikeshoji, and Y. Okamoto, Surf. Sci. **601**, 5237 (2007).
[56] G. Gouy, J. Phys. (France) **9**, 457 (1910).
[57] D. L. Chapman, Philos. Mag. **25**, 475 (1913).
[58] E. Skúlason, G. S. Karlberg, J. Rossmeisl, T. Bligaard, J. Greeley, H. Jónsson, and J. K. Nørskov, Phys. Chem. Chem. Phys. **9**, 3241 (2007).
[59] I. Borukhov, D. Andelman, and H. Orland, Phys. Rev. Lett. **79**, 435 (1997).
[60] I. Borukhov, D. Andelman, and H. Orland, Electrochim. Acta **46**, 221 (2000).
[61] M. Otani and O. Sugino, Phys. Rev. B **73**, 115407 (2006).
[62] R. Jinnouchi and A. B. Anderson, J. Phys. Chem. C (to be published).

[63] J.-L. Fattebert and F. Gygi, J. Comput. Chem. **23**, 662 (2002).
[64] J.-L. Fattebert and F. Gygi, Int. J. Quantum Chem. **93**, 139 (2003).
[65] D. A. Scherlis, J.-L. Fattebert, F. Gygi, M. Cococcioni, and N. Marzari, J. Chem. Phys. **124**, 074103 (2006).
[66] B. Hammer, L. B. Hansen, and J. K. Nørskov, Phys. Rev. B **59**, 7413 (1999).
[67] J. P. Perdew, K. Burke, and M. Ernzerhof, Phys. Rev. Lett. **77**, 3865 (1996).
[68] C. Wohlfarth, in *CRC Handbook of Chemistry and Physics*, 86th ed., edited by D. R. Lide (Taylor & Francis, Boca Raton, 2005), Chap. 6, p. 133.
[69] *CRC Handbook of Chemistry and Physics* (Ref. 68), Chap. 6, p. 127.
[70] A. A. Rashin and K. Namboodiri, J. Phys. Chem. **91**, 6003 (1987).
[71] F. Floris and J. Tomasi, J. Comput. Chem. **10**, 616 (1989).
[72] F. Floris, J. Tomasi, and J. L. Pascual Ahuir, J. Comput. Chem. **12**, 784 (1991).
[73] A. D. Becke, J. Chem. Phys. **88**, 2547 (1988).
[74] B. Delley, J. Chem. Phys. **92**, 508 (1990).
[75] M. J. Frisch *et al.*,GAUSSIAN03, Revision C.02, Gaussian, Inc., Wallingford, CT, 2004.
[76] M. Methfessel and A. T. Paxton, Phys. Rev. B **40**, 3616 (1989).
[77] D. A. McQuarrie, *Statistical Mechanics* (Harper & Row, New York, 1976).
[78] J. Junquera, Ó. Paz, D. Sánchez-Portal, and E. Artacho, Phys. Rev. B **64**, 235111 (2001).
[79] J. M. Soler, E. Artacho, J. D. Gale, A. García, J. Junquera, P. Ordejón, and D. Sánchez-Portal, J. Phys.: Condens. Matter **14**, 2745 (2002).
[80] T. Ozaki and H. Kino, Phys. Rev. B **69**, 195113 (2004).
[81] T. Ozaki and H. Kino, Phys. Rev. B **72**, 045121 (2005).
[82] N. Troullier and J. L. Martins, Phys. Rev. B **43**, 1993 (1991).
[83] L. Kleinman and D. M. Bylander, Phys. Rev. Lett. **48**, 1425 (1982).
[84] D. D. Koelling and B. N. Harmon, J. Phys. C **10**, 3107 (1977).
[85] S. G. Louie, S. Froyen, and M. L. Cohen, Phys. Rev. B **26**, 1738 (1982).
[86] O. Treutler and R. Ahlrichs, J. Chem. Phys. **102**, 346 (1995).
[87] A. H. Stroud, *Approximate Calculation of Multiple Integrals* (Prentice-Hall, Englewood Cliffs, NJ, 1971).
[88] B. Delley, J. Comput. Chem. **17**, 1152 (1996).
[89] P. P. Ewald, Ann. Phys. **64**, 253 (1921).
[90] B. Delley, J. Phys. Chem. **100**, 6107 (1996).
[91] M. Kawata and M. Mikami, Chem. Phys. Lett. **340**, 157 (2001).
[92] A. Brandt, Math. Comput. **31**, 333 (1977).
[93] D. Xie and L. Adams, SIAM J. Sci. Comput. (USA) **20**, 2261 (1999).
[94] J. O'M Bockris and S. U. M. Khan, *Surface Electrochemistry: A Molecular Level Approach* (Plenum, New York, 1993), Chap. 2, p. 78.
[95] C. P. Kelly, C. J. Cramer, and D. G. Truhlar, J. Phys. Chem. B **110**, 16066 (2006).
[96] B. E. Nieuwenhuys and W. H. M. Sachtler, Surf. Sci. **34**, 317 (1973).
[97] B. E. Nieuwenhuys, Surf. Sci. **59**, 430 (1976).
[98] B. E. Nieuwenhuys, D. T. Meijer, and W. H. M. Sachtler, Phys. Status Solidi A **24**, 115 (1974).
[99] J. Hulse, J. Kuppers, K. Wandelt, and G. Ertl, Appl. Surf. Sci. **6**, 453 (1980).
[100] M. Salmeron, S. Ferrer, M. Jazzar, and G. A. Somorjai, Phys. Rev. B **28**, 6758 (1983).
[101] D. M. Collins and W. E. Spicer, Surf. Sci. **69**, 114 (1977).
[102] G. B. Fisher, Chem. Phys. Lett. **79**, 452 (1981).
[103] G. N. Derry and Zhang Ji-Zhong, Phys. Rev. B **39**, 1940 (1989).
[104] J. Clavilier, R. Albalat, R. Gómez, J. M. Orts, J. M. Feliu, and A. Aldaz, J. Electroanal. Chem. **330**, 489 (1992).
[105] V. Climent, B. A. Coles, and R. G. Compton, J. Phys. Chem. **106**, 5988 (2002).
[106] T. Pajkossy and D. M. Kolb, Electrochim. Acta **46**, 3063 (2001).
[107] U. W. Hamm, D. Kramer, R. S. Zhai, and D. M. Kolb, J. Electroanal. Chem. **414**, 85 (1996).
[108] D. E. Peebles and J. M. White, Surf. Sci. **144**, 512 (1984).
[109] C. Nöbl and C. Benndorf, Surf. Sci. **182**, 499 (1987).
[110] K. Bange, T. E. Madey, J. K. Sass, and E. M. Stuve, Surf. Sci. **183**, 334 (1987).
[111] D. L. Price and J. W. Halley, J. Chem. Phys. **102**, 6603 (1995).
[112] A. Kovalenko and F. Hirata, J. Chem. Phys. **110**, 10095 (1999).
[113] E. Gileadi, S. D. Argade, and J. O'M Bockris, J. Phys. Chem. **70**, 2044 (1966).
[114] S. Trasatti, in *Advances in Electrochemistry and Electrochemical Engineering*, edited by H. Gerischer and C. W. Tobias (Wiley, New York, 1977), Vol. 10, p. 213.
[115] H. Ogasawara, B. Brena, D. Nordlund, M. Nyberg, A. Pelmenschikov, L. G. M. Pettersson, and A. Nilsson, Phys. Rev. Lett. **89**, 276102 (2002).
[116] P. Vassilev, R. A. van Santen, and M. T. M. Koper, J. Chem. Phys. **122**, 054701 (2005).
[117] N. M. Marković and P. N. Ross, Jr., Surf. Sci. Rep. **45**, 117 (2002).
[118] H. S. Wroblowa, Y. C. Pan, and G. Razumney, J. Electroanal. Chem. Interfacial Electrochem. **69**, 195 (1976).
[119] S. Mukerjee, S. Srinivasan, M. P. Soriaga, and J. McBreen, J. Phys. Chem. **99**, 4577 (1995).
[120] M. Teliska, V. S. Murthi, S. Mukerjee, and D. E. Ramaker, J. Electrochem. Soc. **152**, A2159 (2005).
[121] M. Shao, K. Sasaki, N. S. Marinkovic, L. Zhang, and R. R. Adzic, Electrochem. Commun. **9**, 2848 (2007).
[122] M. Teliska, V. S. Murthi, S. Mukerjee, and D. E. Ramaker, J. Phys. Chem. C **111**, 9267 (2007).
[123] A. Eichler and J. Hafner, Phys. Rev. Lett. **79**, 4481 (1997).
[124] Ž. Šljivančanin and B. Hammer, Surf. Sci. **515**, 235 (2002).
[125] Th. Heaton and C. Friesen, J. Phys. Chem. C **111**, 14433 (2007).
[126] D. C. Ford, Y. Xu, and M. Mavrikakis, Surf. Sci. **587**, 159 (2005).
[127] X. Lin, N. J. Ramer, A. M. Rappe, K. C. Hass, W. F. Schneider, and B. L. Trout, J. Phys. Chem. B **105**, 7739 (2001).
[128] Y. Y. Yeo, L. Vattuone, and D. A. King, J. Chem. Phys. **106**, 392 (1997).
[129] J. P. Hoare, in *Standard Potentials in Aqueous Solution*, edited by A. J. Bard, R. Parsons, and J. Jordan (Dekker, New York, 1985), Chap. 4, p. 50.
[130] K. P. Huber and G. Herzberg, *Constants of Diatomic Molecules* (Van Nostrand Reinhold, New York, 1979), p. 549.